DISSERTATIONES
PHYSICAE
UNIVERSITATIS
TARTUENSIS
146

MUHAMMAD USAMA JAMAL

Energy transfer to luminescence centres in alkali and rare-earth metal molybdates

DISSERTATIONES PHYSICAE UNIVERSITATIS TARTUENSIS
146

DISSERTATIONES PHYSICAE UNIVERSITATIS TARTUENSIS
146

MUHAMMAD USAMA JAMAL

Energy transfer to luminescence centres in alkali and rare-earth metal molybdates

UNIVERSITY OF TARTU
Press
1632

This study was carried out at the Institute of Physics, University of Tartu, Estonia.

The dissertation was admitted on June 02, 2026, in partial fulfilment of the requirements for the degree of Doctor of Philosophy in Physics, and was allowed for defence by the Scientific Council of the Institute of Physics, University of Tartu.

Supervisors: Dr. Vitali Nagirnõi
Institute of Physics, University of Tartu, Estonia

Dr. Dmitry Spasskiy
Institute of Physics, University of Tartu, Estonia

Opponent: Prof. Gintautas Tamulaitis
Institute of Photonics and Nanotechnology
Vilnius University, Lithuania

Defence: August 25, 2026, at University of Tartu, Estonia

This work has been supported by Estonian Research Council grant PRG2733, the ERDF funding in Estonia granted to the Centre of Excellence TK210 "Centre of Excellence in Sustainable Green Hydrogen and Energy Technologies" and TWINNING project "EXANST" funded by the European Union under grant agreement No. 101159716.

ISSN 1406-0647 (print)
ISBN 978-9908-57-257-4 (print)
ISSN 2806-2523 (pdf)
ISBN 978-9908-57-258-1 (pdf)

University of Tartu Press
www.tyk.ee

CONTENTS

LIST OF PUBLICATIONS INCLUDED IN THE THESIS

I. **M.U. Jamal**, V. Nagirnyi, H. Mändar, K. Chernenko, D. Spassky, Structural and luminescence properties of $K_5Nd(MoO_4)_4$ and $KNd_5(MoO_4)_8$, Journal of Luminescence (2026) 121995. https://doi.org/10.1016/j.jlumin.2026.121995.

II. **M.U. Jamal**, V. Nagirnyi, K. Chernenko, A. Kotlov, Y. Smortsova, D. Spassky, Crystal structure controlled energy transfer to Tb^{3+} in $KTb(MoO_4)_2$ and $K_5Tb(MoO_4)_4$ crystals, Materials Research Bulletin 191 (2025) 113553. https://doi.org/10.1016/j.materresbull.2025.113553.

III. D. Spassky, A. Vasil'ev, **M.U. Jamal**, V.A. Morozov, B.I. Lazoryak, B.S. Redkin, K. Chernenko, V. Nagirnyi, Temperature dependent energy transfer to Eu^{3+} emission centres in $K_5Eu(MoO_4)_4$ crystals, CrystEngComm 26 (2024) 1106–1116. https://doi.org/10.1039/D3CE01201H.

AUTHOR'S CONTRIBUTION

Publication I. The author contributed to setting the physical problem and determining the strategy for conducting experimental research, writing the original draft, manuscript review and editing, experimental work, figure preparation, and data processing and analysis.

Publication II. The author contributed to writing the original draft, manuscript review and editing, experimental work, figure preparation, and data processing and analysis.

Publication III. The author contributed to manuscript review and editing, experimental work, figure preparation, and data processing and analysis.

ABBREVIATIONS

e-h	electron-hole
K5Eu	$K_5Eu(MoO_4)_4$
K5Nd	$K_5Nd(MoO_4)_4$
K5Tb	$K_5Tb(MoO_4)_4$
KNd5	$KNd_5(MoO_4)_8$
KTb	$KTb(MoO_4)_2$
MEE	Multiplication of Electronic Excitation
NIR	Near-Infrared
OPO	Optical Parametric Oscillator
PL	Photoluminescence
PLE	Photoluminescence Excitation
PMT	Photomultiplier Tube
RE	Rare-Earth
RT	Room Temperature
STE	Self-Trapped Exciton
UV-VIS	Ultraviolet-Visible
VUV	Vacuum Ultraviolet

1. INTRODUCTION

Double molybdates containing alkali-metal and rare-earth (RE^{3+}) ions have attracted considerable attention due to their promising luminescence, optical, lasing, magnetic, and scintillation properties [1] [2] [3] [4] [5] [6] [7] [8] [9] [10]. These materials constitute a broad and versatile class of functional inorganic compounds. Their structural flexibility, combined with the unique 4f electronic configurations of RE^{3+} ions, makes them highly suitable for a wide range of photonic and optoelectronic applications.

One of the key advantages of double molybdates is the high tunability of their luminescence properties [11] [12]. Emission and excitation behaviour can be effectively tailored through conventional compositional modification, such as substituting one rare-earth ion for another with a different 4f electronic configuration. For example, replacing Eu^{3+} with Tb^{3+} results in a shift of emission colour from red to green, arising from their distinct electronic structures [11]. In addition, the variation of the alkali-metal cation can significantly influence the crystal structure and the local coordination environment of RE^{3+} ions, thereby modifying the optical response [13].

Beyond the elemental substitution, luminescence properties can also be tailored by modifying stoichiometric ratio of the same elements. Such variations give rise to different crystal structures, leading to changes in the coordination of RE ions, site symmetry, structural ordering, and RE-RE distances. These structural differences play a crucial role in determining energy-transfer pathways and emission efficiency. Compared to the conventional substitution strategies, this approach remains relatively underexplored.

In this work, both strategies for tuning luminescence in double molybdates are systematically investigated. The first approach involves rare-earth ion substitution within the $K_5RE(MoO_4)_4$ system, where Eu^{3+} is replaced by Tb^{3+} or Nd^{3+}. For the second approach, stoichiometrically distinct but elementally identical crystals are compared, specifically $K_5Tb(MoO_4)_5$ (K5Tb) with $KTb(MoO_4)_2$ (KTb) and $K_5Nd(MoO_4)_4$ (K5Nd) with $KNd_5(MoO_4)_8$ (KNd5). Although these compounds contain the same elements, they crystallize in different structures, leading to distinct luminescence behaviours.

A detailed understanding of how stoichiometric ratio driven structural variations influence luminescence properties, particularly in double molybdates, remains limited compared to that of elemental substitution, which is widely reported to tune the emission properties of these materials [11] [12] [14]. Therefore, in this work, a systematic investigation using both approaches is conducted to establish a structure-property relationship governing energy-transfer processes and luminescence properties of double molybdates, as well as the changes induced by RE^{3+} ion substitution. A comprehensive understanding of these relationships enables the development of more efficient, application-specific photonic materials.

To elucidate the changes in luminescence properties arising from these modifications, a systematic photoluminescence (PL) spectroscopy study is performed.

PL spectroscopy provides key information on emission wavelengths, excitation mechanisms, luminescence lifetimes, and thermal quenching behaviour, as well as insights into energy-transfer processes. The use of synchrotron radiation for luminescence spectroscopy enabled us to expand research into the deep VUV region.

In RE^{3+} based double molybdates, excitation can occur via both intracentre and interband mechanisms. In intracentre excitation, electrons are excited within the 4f levels of the RE^{3+} ions, followed by radiative or non-radiative relaxation to the lower emitting states. In interband excitation, energy is first absorbed by the MoO_4 complex, typically via transition of electrons from the 2p oxygen states forming the top of the valence band to the 4d molybdenum states forming the bottom of the conduction band, and subsequently transferred to the RE^{3+} ions. During this process, intermediate phenomena such as inelastic scattering with creation of secondary e–h pairs, interactions with lattice vibrations (thermalization), exciton formation and charge-carrier trapping may occur. These processes noticeably influence the efficiency and pathway of energy transfer to the emitting centres. Therefore, understanding the energy transfer processes is essential for identifying the factors governing luminescence and for optimizing the optical performance of these materials.

The main aim of the thesis is:

- To investigate the influence of elemental composition and structural arrangement of potassium rare earth double molybdates on their luminescence properties, electronic band structure, and processes of energy transfer to the luminescence centres.

To achieve the aim, the following tasks were performed:

1. Measurement of XRD patterns to characterize the crystal.
2. Measurements of the absorption and reflection spectra to elucidate modifications of band structure and identify intracentre 4f–4f RE^{3+} transitions.
3. Measurement of emission spectra over a wide UV-NIR spectral range to identify the characteristics of emission centres.
4. Photoluminescence excitation (PLE) spectroscopy in the 2.5–45 eV range to clarify the mechanisms of energy transfer to emission centres.
5. Determination of lifetimes of emitting states and investigation of thermal quenching processes using temperature-dependent decay kinetics and luminescence intensity measurements.

2. GENERAL BACKGROUND

2.1. Overview of energy transfer processes in luminescent materials

Energy transfer in luminescent ionic crystals is a multi-stage process initiated by interaction with ultraviolet (UV), vacuum ultraviolet (VUV), or ionizing radiation [15]. A pictorial representation of relaxation processes is shown in Fig. 1. Absorption of high-energy radiation generates primary, highly energetic charge carriers such as hot electrons excited high into the conduction band and holes created in the valence band or in core electronic states. Hot electrons undergo rapid inelastic electron–electron scattering, during which their primary excess kinetic energy is transferred to the electrons in the valence band, generating secondary electron-hole pairs in the material. The multiplication of electronic excitations continues until the electron energy drops below the electron-electron scattering threshold. Simultaneously, deep core holes relax through Auger processes. In this mechanism, an electron from the valence band moves to the core state hole, and the released energy is transferred non-radiatively to another electron, which is subsequently excited into the conduction band as an Auger electron. The combined inelastic scattering and Auger relaxation processes lead to rapid redistribution and multiplication of electronic excitations on ultrafast timescales of approximately 10^{-15}–10^{-16} s, while the total energy of the electronic subsystem remains nearly conserved.

The next stage is the thermalization of excited carriers through interaction with the crystal lattice. During this process, hot electrons and holes lose excess kinetic energy via phonon emission and relax toward the bottom of the conduction band and the top of the valence band, respectively. A substantial fraction of the absorbed energy is transferred to the lattice as vibrational energy.

After thermalization, depending on the material's lattice properties, the thermalized carriers may form self-trapped excitons (STEs), localize at defects, or be captured by impurity and luminescence centres during migration. These migration-stage interactions strongly influence the efficiency of energy transfer and luminescence formation. In rare-earth-doped materials, energy transfer from the host lattice to the 4f states of activator RE ions occurs via sequential capture of separated electrons and holes, or via the intermediate formation of excitonic states.

The final stage of energy relaxation involves radiative and non-radiative recombination. In radiative relaxation, the stored excitation energy is emitted as luminescence photons, whereas non-radiative processes dissipate energy into the lattice through phonon emission.

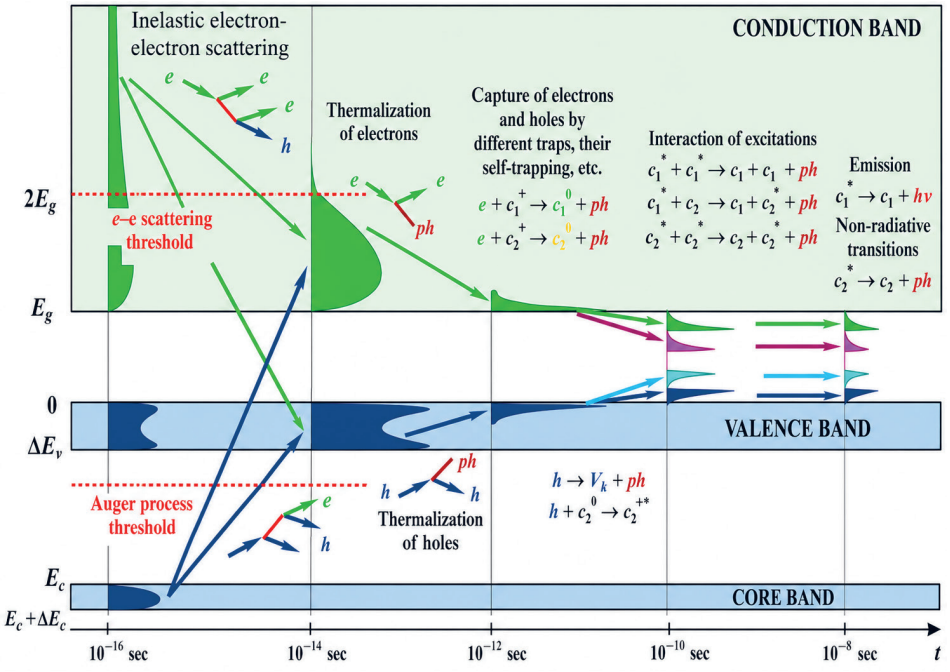

Figure 1: Scheme of relaxation of electronic excitations in an intrinsic scintillator. e = electrons, h=holes, ph=phonons, *hv*= photons, V_k = self-trapped holes, c_n = ionic centres with charge n [15].

2.2. Overview of double molybdates

To date, many double molybdate compounds have been synthesized and structurally characterized in detail [1] [11] [14] [16] [17] [18]. In addition, a scheme has also been derived for $KRE(MoO_4)_2$ type double molybdates, providing a systematic description of the relative positions of the RE^{3+} energy levels with respect to the valence and conduction bands [19]. This scheme provides important insight into luminescence processes in double molybdates. In particular, the energy gap between the excited 5d levels of RE^{3+} ions and the bottom of the conduction band determines the thermal stability of the emission centres, since small gaps facilitate thermal ionization and luminescence quenching. Furthermore, analysis of the energy positions of the ground and excited 4f states helps clarify the mechanisms of host-to-RE energy transfer. When these 4f states are located close to or overlap with the valence or conduction bands, direct sequential capture of separated electrons and holes by the RE^{3+} ions becomes inefficient due to competing carrier thermalization processes in the lattice. Under these conditions, energy transfer from the host lattice to the rare-earth ions is expected to occur predominantly via intermediate excitonic states. According to the scheme proposed in [19], this mechanism is expected to dominate in the studied potassium double molybdates with RE = Eu, Tb, and Nd.

The crystals studied in this work, such as $K_5Eu(MoO_4)_4$ (K5Eu), $K_5Tb(MoO_4)_4$, $K_5Nd(MoO_4)_4$ and $KTb(MoO_4)_2$, have also been investigated previously from a crystallographic perspective, and information on phase formation, crystal symmetry, lattice parameters, and the coordination environments of the rare-earth ions is already known [8] [9] [11] [1] [20]. The luminescence properties of these compounds have not been investigated in detail. In many cases, general spectroscopic experiments were performed, including recording emission spectra under the most intense excitation line to illustrate the main emission from the samples, measuring its excitation spectra in the conventional UV-Vis range and luminescence decay kinetics. However, comprehensive studies of excitation mechanisms, energy transfer processes, site-selective luminescence, luminescence thermal quenching, electron relaxation mechanisms within the 4f states of RE^{3+}, and secondary excitation creation under high-energy excitation remain largely absent.

Among the different structural families of double molybdates, compounds crystallizing in the $MRE_5(MoO_4)_8$ form remain particularly underexplored. Many possible alkali metal-rare-earth combinations in this structural type have not yet been reported, such as $KNd_5(MoO4)_8$, leaving the influence of stoichiometric ratio driven structural variations on optical properties insufficiently understood. Therefore, significant gaps also remain in understanding how crystal structure, local symmetry, and RE-RE distances influence the optical and luminescence properties of these materials.

The present work aims to partially fill these gaps by conducting a comprehensive investigation of the luminescence properties and energy-transfer processes in selected potassium rare-earth molybdate crystals. Particular emphasis is placed on comparing intracentre and interband excitation processes and on analyzing how these excitation pathways affect emission spectra, luminescence decay kinetics, and the thermal stability of luminescence. Furthermore, to obtain deeper insight into the local environment of the rare-earth ions, high-resolution emission and excitation spectroscopy were employed. In addition, site-selective luminescence studies were performed to distinguish the optical behaviour of different rare-earth centres present in the crystals. Another important aspect of this work is the use of powerful excitation sources, including an optical parametric oscillator (OPO) laser and synchrotron radiation, for recording emission and excitation spectra over a broad energy range. Unlike conventional excitation sources such as xenon or deuterium lamps, these high-intensity excitation methods enable the observation of emissions from higher-lying 4f excited states that are normally inaccessible or too weak to detect. As a result, additional radiative and non-radiative relaxation channels can be identified and analysed in detail. Furthermore, excitation spectra measured under synchrotron radiation over the wide energy range of 4–45 eV provide important insight into high-energy excitation processes and energy-transfer mechanisms in these materials.

Overall, this work extended the current understanding of alkali rare-earth molybdates by moving beyond structural characterization to a detailed spectroscopic investigation of their luminescence properties and energy-transfer mechanisms.

3. METHODOLOGY

3.1. Preparation of the samples

The crystals investigated in this work were grown using the Czochralski technique under similar experimental conditions. Therefore, the detailed crystal growth procedure is described only for the KTb crystal as a representative example to illustrate the synthesis methodology employed for all the investigated crystals. The exact crystal growth details of the individual crystal can be seen in the following references [9] [11] [1]. The polycrystalline materials used to grow the KTb single crystal were synthesized by solid-state reaction. A stoichiometric mixture of the reagents (K_2CO_3, Tb_4O_7 of spectroscopic purity ≥99.995%, and MoO_3) was annealed in a Pt crucible at 773−823 K for 15 h to decompose the carbonate. After that, the mixture was ground, homogenized, and heated at 1173 K for 15 h in air. The synthesized polycrystalline material was melted in a 40 mm diameter Pt crucible using an induction furnace operating at 17 kHz. A small-sized bar of non-oriented KTb single-crystal was used as a seed. The growing temperature was accurately determined by repeated seeding trials. A KTb colourless, transparent crystal with a diameter of up to 10 mm and a length of 20 mm was grown at 1373 K by the Czochralski technique at a pulling rate of 0.5–1.5 mm/h and a rotation rate of 50 rpm in a slightly oxidizing atmosphere [9].

3.2. Photoluminescence spectroscopy techniques

Photoluminescence spectroscopy is an essential experimental technique for investigating energy transfer processes and the luminescence properties of phosphors. It provides direct information on electronic transitions, emission mechanisms, and relaxation processes in luminescent materials. In this work, different PL spectroscopy setups were employed depending on the specific aim of each investigation. The details of these experimental setups are given below:

- The spectral measurements under excitation in the 2–6 eV energy range were performed at the UV-Vis setup in Tartu. Two types of lamps served as excitation sources: a 400-W deuterium discharge lamp (DDS-400) was used to measure excitation and emission spectra, whereas a PerkinElmer 150-W xenon pulsed flash lamp (1 μs) was used for decay kinetics. Both excitation sources are used in combination with a primary double-quartz prism monochromator (DMR-4). The samples were mounted in a Janis VPF-800 liquid nitrogen cryostat (65–800 K) either by conductive silver glue or by a screw-tightened copper clip. Emission spectra were recorded using a secondary ARC Spectra Pro 308i Czerny-Turner-type grating monochromator equipped with a photomultiplier tube H8259-01. Different SCHOTT glass filters were used to eliminate second-order excitation and emission in the secondary monochromator. Excitation and emission spectra were measured at room

temperature and at 78 K. A LakeShore 335 temperature controller was used to monitor temperature and control crystal heating. The experimental setup was operated using a LabView software.

- For excitation in the 3–11 eV region, a VUV system comprising a deuterium discharge lamp and a Seya Namioka McPherson 234/302 monochromator equipped with a 300 gr/mm grating (dispersion 16 nm/mm, optimized for 160 nm) was used. The samples were mounted on a sample holder of a closed-cycle helium cryostat from ARS (Advanced Research Systems, Inc.). The primary monochromator and cryostat were under a high vacuum of 7×10^{-7} mbar, maintained by a turbomolecular pump. The emission spectra were recorded using an Andor Shamrock 303i-B grating monochromator equipped with a CCD detector (Andor iDus 416) or with various photo-multiplier tubes Hamamatsu H8259, H8259-01, or H8259-02. All measurements were carried out over the temperature range 5-350 K controlled using a LabView software.
- PL spectra and decay curves were also measured using a tunable optical parametric oscillator NT242, which provided excitation wavelength selection across 210–2600 nm with a 3-ns pulse duration. The samples were mounted in a Janis VPF-800 cryostat, allowing temperature control from 77 to 800 K using a Lake Shore 335 temperature controller. Depending on the measurement conditions, the emission spectra were recorded using either an Andor Shamrock 303i-B or a Kymera 328i spectrograph, coupled to a CCD detector. Decay curves were recorded using Hamamatsu R3377 and Hamamatsu H10330A-75 NIR-PMT detectors, sensitive in the UV-Vis and NIR regions, respectively, coupled to a LeCroy 6100A 1 GHz oscilloscope.
- Luminescence and PLE spectra with high spectral resolution were recorded using a specialized laboratory setup with an ARC 150 W Xe lamp as the excitation source. The excitation wavelength was selected using an MDR-206 monochromator equipped with a 1200 gr/mm grating (dispersion 4.2 nm/mm). The excitation spectra were measured with a spectral resolution of 0.4 nm. The samples mounted in a vacuum optical cryostat (Cryotrade LN-120) were studied over the temperature range of 77–500 K. Temperature was controlled using a LakeShore 335 controller. The luminescence spectra were recorded with a spectral resolution of 0.32 nm using an Oriel MS257 spectrograph with a 2400 gr/mm grating (dispersion 1.6 nm/mm), equipped with a Marconi 30–11 CCD detector.
- PLE spectra in the UV-VUV range (3.7–40 eV) were recorded at the P66 beamline of the PETRA III storage ring at DESY [21]. The excitation energy was selected using a 2 m McPherson monochromator equipped with two interchangeable holographic concave gratings (1200 gr/mm) coated with Pt and Al+MgF_2. The Al+MgF_2 coated grating was optimized for the 3.75–11 eV spectral range, while the Pt-coated grating was used for measurements at higher excitation energies. The excitation spectra were measured with a

spectral resolution of approximately 0.5 nm (corresponding to ~0.06 eV at 12 eV). The samples were mounted in a flow helium cryostat, which allowed them to cool to 10 K. The emitted luminescence was analysed using an ANDOR Kymera 328i monochromator and detected with a Hamamatsu R6358 photo-multiplier tube. The PLE spectra were normalized to the luminescence yield of sodium salicylate.

- PL studies including emission, excitation and reflection spectra in the excitation energy range 4.5 – 45 eV were also conducted at the photoluminescence end station of the FinEstBeAMS beamline at the 1.5 GeV storage ring of the MAX IV synchrotron facility [22] [23]. The photon source for FinEstBeAMS is an in-house-built, elliptically polarized undulator (EPU) of the APPLE II type, which provides tunable photon energies from the ultraviolet to the soft X-ray range (4.5–1300 eV). Depending on photon energy, the photon flux varies from 1×10^{11} to 8×10^{13} ph/s. The generated beam is collimated by a toroidal mirror (M1) and directed to the input of a grazing-incidence primary monochromator equipped with a 92 lines/mm grating (See Fig.2), providing a photon-energy resolution of approximately 2.3 meV at 10 eV. To suppress higher-order excitation radiation from the grating, an appropriate set of optical filters was employed, depending on the first-order excitation energy. These included fused silica and MgF_2 optical filters, as well as thin metallic films of In, Sn, Mg, and Al. The excitation spectra were subsequently corrected for the reference signal of a factory-calibrated AXUV-100G diode. The crystals were mounted in an ARS closed-cycle helium cryostat. To measure reflectivity spectra, the radiation reflected by the sample at an angle of 22.5° fell on a screen made of sodium salicylate, which has a constant light yield, and the salicylate emission was registered by a Hamamatsu H11123 counting head. PL excitation spectra were obtained by recording emission spectra with a CCD camera at different excitation energies, thereby covering the 300 nm range in a single scan. Time-resolved measurements were performed in single-bunch operation mode. In this mode, the duration of a single excitation pulse was ~160 ps, with a 320 ns gap between pulses. The luminescence signal was re-corded using an optical fiber-coupled Andor Shamrock SR-303i spectrometer equipped with a thermoelectrically cooled hybrid photodetector, HPM-100-07C, from Becker & Hickl. For steady-state measurements, a Newton CCD camera (Andor, model DU970P-BVF) was used in multi-bunch mode. The spectra were corrected for the registration system’s spectral sensitivity function.

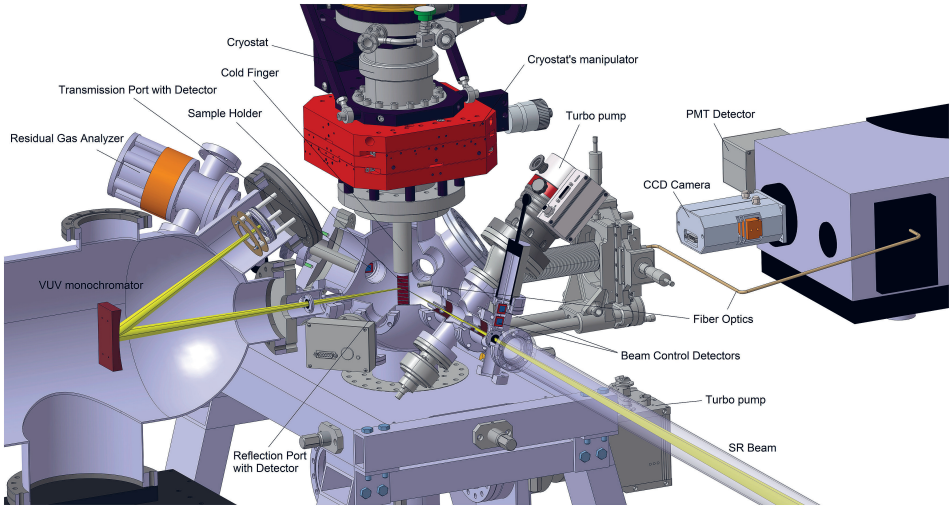

Figure 2: A scheme of the photoluminescence setup at the FinEstBeAMS beamline [22].

4. RESULTS AND DISCUSSION

This section presents a comparative study of the energy transfer mechanism and luminescence properties of RE^{3+} ions (RE = Eu, Tb, Nd) in the $K_5RE(MoO_4)_4$ system, along with crystals of identical elemental composition but different crystal structures, namely $KRE(MoO_4)_2$ (RE = Tb) and $KRE_5(MoO_4)_8$ (RE = Nd). The objective is to show how substituting RE^{3+} ions and varying the crystal structure influence the energy-transfer processes and luminescence properties of these ions.

A particular emphasis is placed on several key aspects. The fine structure of the emission lines is analysed, with special attention to how differences in the point symmetry of RE^{3+} and its nearest environment influence spectral line shapes and splitting patterns of emissions originating from the 4f states of RE^{3+} ions. Moreover, the influence of crystal structure on electronic band structure is investigated, providing insight into band structure engineering of the material. In addition, the effect of structural differences on luminescence decay kinetics is investigated, highlighting variations in radiative and nonradiative relaxation processes. The mechanisms responsible for thermal quenching of luminescence are also discussed, with a focus on how distinct lattice environments affect the thermal stability of the excited states.

4.1. Crystal structure

Most $M_5RE(MoO_4)_4$ compounds crystallize in the R3m space group, similar to the $K_2Pb(SO_4)_2$ type palmierite structure [24] [25]. Palmierite-related phases can be generally described by the formula $M2M1(AO_4)_2$, consisting of alternating M2 layers and $[M1A_2O_8]$ layers stacked along the c-axis of the rhombohedral unit cell. In this structure, the M2 and M1 cations are arranged in distinct layers. The M2 sites are exclusively occupied by M^+ cations, whereas the M1 sites are occupied by either RE^{3+} ions or M^+ ions in statistical alternation depending on the elemental composition. The crystal structure may exhibit various distortions depending on the constituent element. These distortions are mainly associated with the rotations of the MoO_4^{2-} tetrahedra and with the ordering of RE^{3+} and M^+ cations at the M1 sites. Due to the structural flexibility of the MoO_4 tetrahedral units, different coordination environments for RE^{3+} ions can be stabilized within the lattice. Ordering of RE^{3+} and M^+ cations at the M1 sites plays a crucial role in determining the overall crystal symmetry. In particular, ordering between M^+ and RE^{3+} cations can reduce symmetry from the ideal rhombohedral R3m to lower symmetry. Depending on the degree and nature of cation ordering, the structure may transform into a monoclinic phase (e.g., C2/c) or even into an incommensurately modulated monoclinic phase described by a superspace group such as X2/m(0β0)00. Such symmetry-lowering due to cation ordering at the M1 site demonstrates that the palmierite-type structure is highly flexible, allowing it to accommodate cations of different sizes while maintaining structural stability.

It has been shown that the crystal structure of both K5Eu and K5Tb crystals can be refined using the Rietveld method within the framework of a (3+1)D incommensurately modulated structure described by the superspace group C2/m(0β0) [11] [1]. In K5Eu, the local environments of K1 and Eu^{3+} sites are only weakly affected by the rotations of the MoO_4^{2-} tetrahedra and shifts of oxygen atoms, resulting in eightfold coordination for both K1 and Eu^{3+}. In contrast, the local structure around the K1 and Tb^{3+} sites in K5Tb is strongly influenced by the rotations of the MoO_4^{2-} tetrahedra and displacements of oxygen atoms. Consequently, the coordination environments are significantly distorted, leading to coordination numbers ranging from 6 to 10. In $K_5RE(MoO_4)_4$, the distance between the two nearest RE^{3+} is approximately 6 Å [8] [1].

$KTb(MoO_4)_2$ has an orthorhombic structure, indexed in the Pbcn space group [9] [14]. The structure consists of layers, formed by the $[TbMo_2O_8]$ units, which include the TbO_8 polyhedra and MoO_4 tetrahedra. These layers are oriented perpendicular to the b-axis and are separated by zigzag layers of K^+ ions. Neighboring TbO_8 polyhedra share edges, forming infinite $[Tb_2O_{14}]_n$ chains along the c-axis, with a Tb-Tb distance of about 4 Å within the chains [9] [16]. The MoO_4 tetrahedra separate these chains, causing a one-dimensional arrangement of Tb^{3+} ions.

Powder X-ray diffraction characterization showed that K5Nd crystal indexing was equally possible in both the trigonal and monoclinic space groups. The base structure of the K5Nd crystal can be described in a trigonal system, consisting of three distorted $(K,Nd)O_6$ octahedra and six distorted MoO_4 tetrahedra. K and Nd share the 3a Wyckoff position (site symmetry notation "–3m"). The distance between the two nearest Nd atoms is approximately 5.98 Å. The monoclinic crystal system allows for an ordered distribution of K and Nd at the M positions of a palmierite-type structure.

The crystal structure of KNd5 belongs to the family of incommensurately modulated scheelite-type structures described within the (3+1)D superspace group I2/b(αβ0)00. In this structure, Nd^{3+} ions are coordinated by eight oxygen atoms, forming NdO_8 coordination polyhedra. The K^+ and Nd^{3+} cations incommensurately share the 4e Wyckoff position located on a second-order rotation axis (site symmetry 2). The shortest Nd-Nd distance in the structure is approximately 4 Å.

4.2. Photoluminescence properties

4.2.1. Emission spectra

4.2.1.1. Effect of RE^{3+} substitution on emission characteristics

The PL spectra of K5Eu, K5Tb, and K5Nd crystals measured under 45 eV excitation to demonstrate the effect of RE^{3+} ion substitution on emission characteristics are depicted in Fig. 3. This high excitation energy corresponds to the interband transitions from the valence band or core levels to the conduction band,

allowing excitation of the whole set of emission centres in the crystals. The K5Tb crystal displayed emission lines in the 370–640 nm range, which resulted from the 4f-4f transitions in Tb^{3+}, see energy level scheme in Fig. 4. The weak blue emission lines in the 370–480 nm region were associated with transitions from the $^5D_3$ level to the ^7F_J ground states, whereas the more intense emissions in the 480–640 nm region originated from the $^5D_4$ level to the ^7F_J (J = 3–6) levels. The most prominent emission was observed at 545 nm, corresponding to the $^5D_4 – {}^7F_5$ transition, responsible for the characteristic green luminescence of Tb^{3+}.

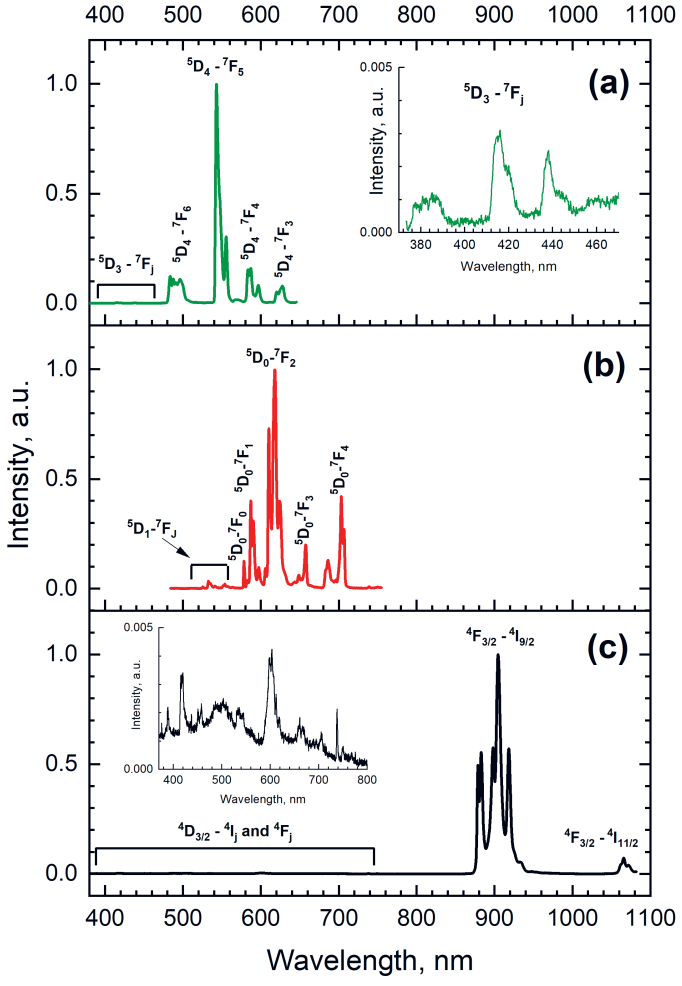

Figure 3: Luminescence spectra of $K_5Tb(MoO_4)_4$ (a), $K_5Eu(MoO_4)_4$ (b) and $K_5Nd(MoO_4)_4$ (c) measured under excitation 45 eV at T = 7 K.

In contrast, the K5Eu crystal exhibited a series of sharp emission lines in the 520–720 nm range arising from intraconfigurational 4f-4f transitions of the Eu^{3+} ion. The emissions observed in the 580–720 nm region are attributed to transitions from the $^5D_0$ excited state to the ^7F_J (J = 0–4) levels, with the most intense peak at 618 nm corresponding to the $^5D_0 - {}^7F_2$ transition, giving rise to strong orange-red luminescence. Relatively weaker bands in the 520–570 nm region originated from higher excited states $^5D_1$ and $^5D_2$, which undergo partial radiative relaxation to the ground state before non-radiative decay to the $^5D_0$ level.

In the Nd^{3+} substituted crystal (K5Nd), the emission characteristics change significantly, dominated by an intense near-infrared (NIR) emission arising from the $^4F_{3/2}$–$^4I_{9/2}$ and $^4F_{3/2}$–$^4I_{11/2}$ transitions within the $4f^3$ configuration of Nd^{3+}. In addition to these strong NIR lines, weak but distinct emission lines are observed in the visible region, which are rarely reported for Nd^{3+} systems. These emissions are detectable under high excitation density, when higher-lying 4f levels become sufficiently populated. The observed visible emission lines are assigned to the $^4D_{3/2}$–$^4I_{11/2}$ (388 nm), $^4D_{3/2}$–$^4I_{13/2}$ (420 nm), $^4D_{3/2}$–$^4I_{15/2}$ (460 nm), $^2P_{3/2}$–$^4I_{15/2}$ (504 nm), $^4D_{3/2}$–$^4F_{3/2}$ (612 nm), $^4D_{3/2}$–$^4F_{5/2}$+$^2H_{9/2}$ (655 nm), $^4D_{3/2}$–$^4F_{7/2}$+$^4S_{3/2}$ (700 nm), and $^2P_{3/2}$–$^4F_{5/2}$+$^2H_{9/2}$ (770 nm) transitions. Overall, the results clearly demonstrate that substituting different RE^{3+} ions into the $K_5RE(MoO_4)_4$ crystal significantly shifts the emission wavelength, with Tb^{3+} yielding strong green emission, Eu^{3+} giving intense orange-red emission, and Nd^{3+} exhibiting dominant NIR emissions.

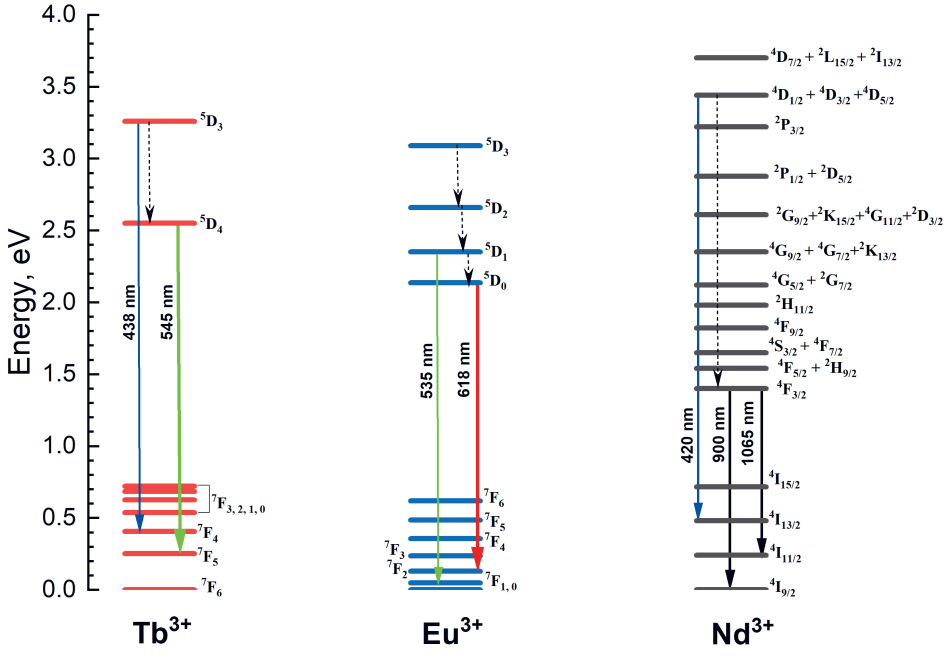

Figure 4: Energy level scheme of Tb^{3+}, Eu^{3+}, and Nd^{3+}.

4.2.1.2. Effect of structural variation on emission characteristics

Comparative studies of the photoluminescence of crystals with identical elemental composition but different crystal structures to understand the influence of structural variation on luminescence properties were performed on Tb^{3+} and Nd^{3+} based crystals. A pronounced dependence of the emission characteristics on crystal structure was observed, particularly between the K5Tb/KTb and K5Nd/KNd5 crystals.

The fine structure of the 4f electronic transitions was analysed in detail, allowing the observation of Stark splitting patterns associated with crystal-field interactions. Such measurements are particularly important because the spectral fine structure is highly sensitive to local symmetry, crystal-field strength, and structural distortions around the RE^{3+} ions. Consequently, high-resolution spectroscopy provides valuable information regarding the occupation of crystallographic sites and the local coordination environment within the crystal lattice.

For the Tb^{3+} based materials, the most intense emission in the 540–560 nm spectral range, corresponding to the $^5D_4$–$^7F_5$ transition, was analysed in detail by recording high-resolution (0.4 nm) emission spectra for two potassium terbium molybdates exhibiting different crystal structures, KTb and K5Tb (Fig. 5). A noticeable difference in spectral line shape and fine structure of the emission spectra was observed for these two crystals. The ordered KTb crystal, in which Tb^{3+} ions occupy TbO_8 polyhedra, exhibited a well-resolved fine structure consisting of 11 fine spectral lines. The appearance of the 11 resolved lines in KTb is consistent with the maximal crystal field splitting of the $^7F_5$ multiplet into Stark levels, given by the 2J+1 rule in the case of a completely lifted degeneracy. The observation of the complete set of the emission lines in KTb therefore indicates a highly ordered local environment of Tb^{3+} ions preferentially occupying one type of sites, in which the crystal field is sufficiently well defined to fully resolve the Stark splitting of the emitting level.

In the case of K5Tb, the emission lines were significantly smeared, suggesting a more complex, less uniform local crystal-field environment for the Tb^{3+} ions. Structural analysis indicates that the Tb^{3+} ions are coordinated by oxygen atoms in K5Tb, forming coordination polyhedra ranging from TbO_6 to TbO_{10}. Such variability in coordination geometry leads to inhomogeneous broadening due to the overlapping of emission lines from multiple emitting centres.

Since multiple crystallographic sites may coexist in these materials, conventional luminescence spectra often consist of overlapping contributions from several emitting centres. Site-selective excitation enables probing of individual RE^{3+} sites and thus provides a more detailed understanding of site-dependent emission behaviour.

To distinguish between the broadening arising from multiple crystallographic sites and that originating from structural disorder, the emission spectra were measured at 78 K by selecting the excitation energy in the 2.54–2.59 eV range, which corresponds to the broad line in excitation spectra arising due to the $^7F_6$–$^5D_4$ Tb^{3+} transitions (see Fig. 8). The results showed that the emission

profile remained consistently broadened without the emergence of additional resolvable site-specific features. This behaviour confirms that the observed spectral broadening in K5Tb is primarily determined by structural disorder rather than by the overlapping of emission lines originating from multiple non-equivalent Tb^{3+} sites.

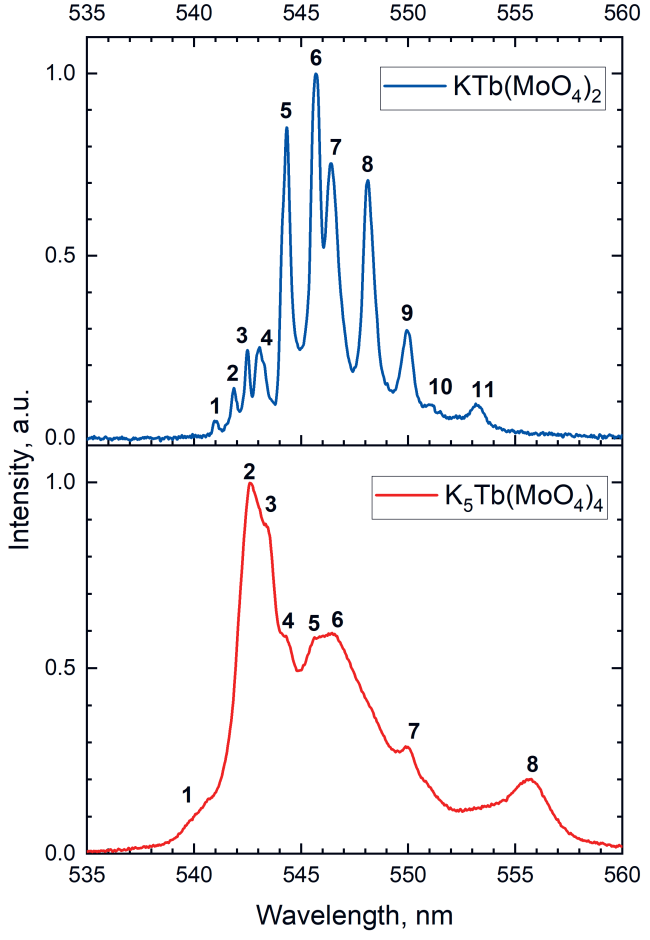

Figure 5: Luminescence spectra in the region of the $^5D_4$–$^7F_5$ transitions in KTb and K5Tb measured under excitation 2.55 eV, at T = 78 K.

Similarly, crystal field splitting of the $^4I_{9/2}$ state of Nd^{3+} ions in K5Nd and KNd5 showed pronounced differences, as depicted in Fig. 6. In K5Nd, the lines related to the transitions from the $^4F_{3/2}$ state to different Stark components of the $^4I_{9/2}$ state are observed within the 875–930 nm spectral range, whereas they form two distinct groups divided by a gap at about 890 nm. In KNd5, the corresponding group of lines is slightly shifted to the shorter wavelength range 860–930 nm, and the spectral positioning of the first four lines is more compact. Also, a distinct

redistribution of emission intensity between lines associated with different Stark levels is observed in the two crystals, which confirms that Nd^{3+} ions experience distinct local crystal-field environments in the two compounds, likely due to variations in site symmetry and coordination geometry in NdO_6 octahedra and NdO_8 polyhedra, hosting the Nd^{3+} ions in K5Nd and KNd5, respectively, which affect both energy splitting and transition probabilities.

The emission lines' width is similar in both crystals, indicating a similar level of structural disorder, contrary to the findings in potassium terbium molybdate crystals, where the emission lines of Tb^{3+} are substantially broadened in $K_5Tb(MoO_4)_4$ compared to those in $KTb(MoO_4)_2$ due to higher structural disorder in the former crystal [26].

Overall, these findings clearly demonstrate that RE^{3+} substitution and stoichiometric ratio driven structural changes noticeably influence the spectral characteristics of RE^{3+} emissions in double molybdates.

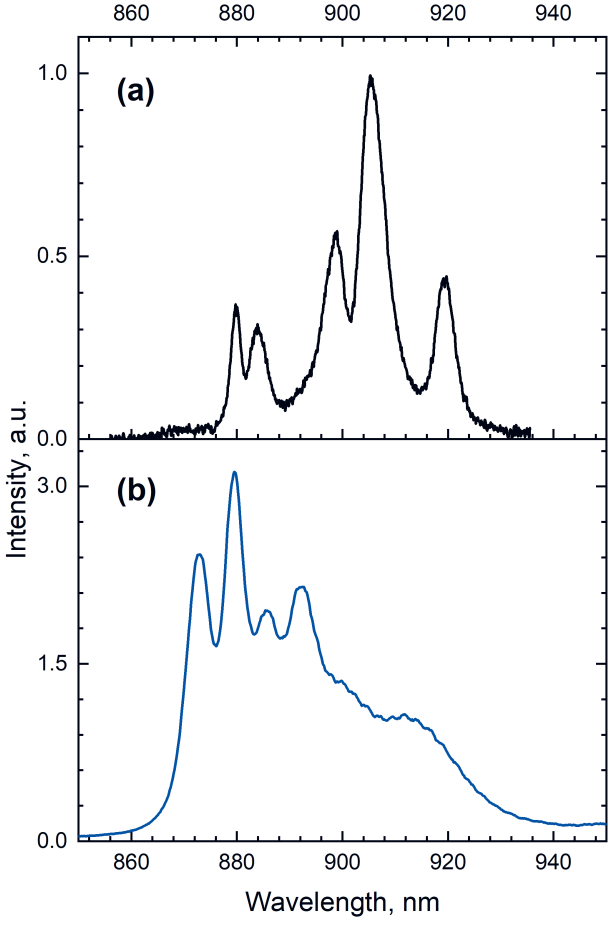

Figure 6. Luminescence spectra in the region of the $^4F_{3/2} - {}^4I_{9/2}$ transitions in $K_5Nd(MoO_4)_4$ (a) and $KNd_5(MoO_4)_8$ (b) measured under excitation 4.5 eV at T = 78 K.

4.2.2. Photoluminescence excitation

Photoluminescence excitation spectra provide substantial information about the energy-level structure of materials involved in luminescence processes and are essential for selecting suitable excitation energies to investigate various relaxation mechanisms. To evaluate the influence of RE^{3+} ion substitution and crystal structure on excitation characteristics, PLE spectra of all investigated crystals were measured over a wide excitation-energy range from 2.5 eV to deep VUV range (typically 45 eV) (Fig. 7). All studied crystals exhibit a broad excitation band in the 4–8 eV region, attributed to interband electronic transitions from the 2p O states at the top of the valence band to the 4d Mo states at the bottom of the conduction band. The presence of this broad band demonstrates efficient energy transfer from the MoO_4^{2-} complex to the RE^{3+} ions in all compounds. Since the broad excitation band appears at nearly the same spectral position in all $K_5RE(MoO_4)_4$ crystals, this indicates that the substitution of the RE^{3+} ion does not significantly modify the electronic structure of the MoO_4^{2-} complex within this crystal family. The bandgap variations are within 0.3 eV, depending on the composition. In contrast, substantial differences are observed in the crystal transparency region (2.5–4 eV), where narrow excitation lines corresponding to intra-configurational 4f-4f transitions of RE^{3+} ions are present. Variations in the position, intensity, and number of these excitation lines arise from the different electronic configurations and 4f energy-level schemes of the individual rare-earth ions as well as crystal structure modifications.

To investigate the effect of crystal structure on excitation mechanisms, the PLE spectra of K5Tb were compared with those of KTb, and K5Nd with KNd5, over the same wide energy range (2.5–45eV). In both Tb^{3+} and Nd^{3+} based crystals, noticeable differences were observed in the spectral pattern, linewidth, and intensity of the 4f-4f excitation lines (Fig. 7). These variations are associated with differences in the local symmetry, coordination environment of the RE^{3+} ions, and the degree of structural ordering resulting from different crystal stoichiometries.

A pronounced structural effect was observed for the Tb^{3+} based crystals in the excitation lines associated with the $^7F_6$–$^5D_4$ transitions of Tb^{3+} (Fig. 8). In ordered KTb crystal, a well-resolved fine structure of the excitation lines is clearly visible, whereas in partially disordered K5Tb crystal, significant spectral broadening and smearing are observed. In addition to changes in the line shape, clear differences also appear in the position of the absorption edge and in the maximum of the broad excitation band, indicating the increase of the bandgap by 0.3 eV in K5Tb (Fig.7).

In the case of Nd^{3+} based crystals, comparison of the PLE spectra of K5Nd and KNd5 (Fig. 7d and 7e) also revealed noticeable differences in the spectral fine structure and linewidth of the 4f–4f transitions. These differences similarly originate from variations in local symmetry and coordination environments around Nd^{3+} ions in the two crystal structures. However, unlike the Tb based molybdates, the crystal structure does not appear to significantly influence the bandgap in Nd based compounds, as evidenced by the broad excitation bands occurring at nearly identical energies in both crystals and reflectivity spectra measurements.

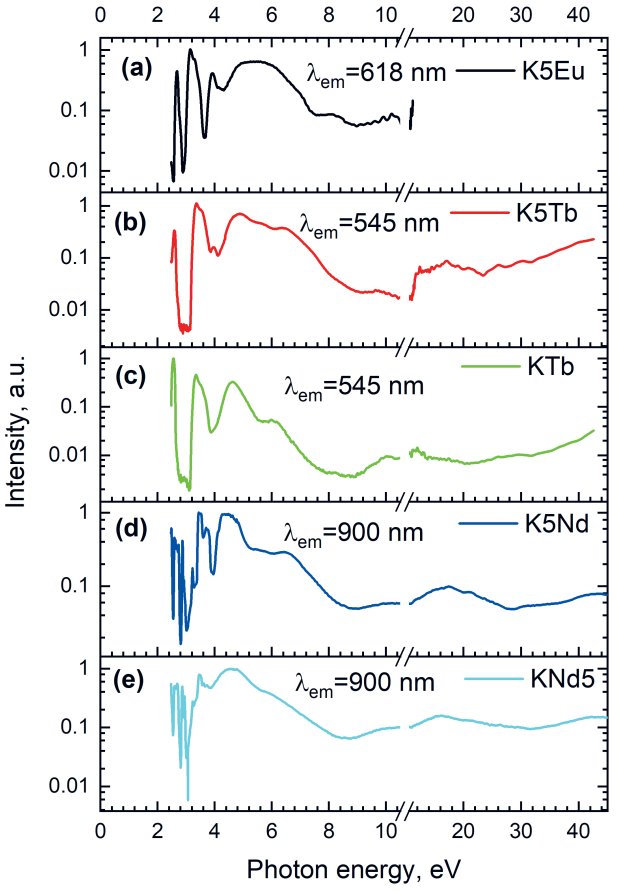

Figure 7: Photoluminescence excitation spectra of potassium rare earth double molybdates in semilogarithmic scale measured at 7 K.

The high-energy region of the excitation spectra provides further insight into energy-transfer processes involving free charge carriers. In particular, it is shown that the structural disorder influences the efficiency of energy transfer from the separated e–h pairs to RE^{3+}. At excitation energies above approximately 5.5 eV, typically separated electron-hole pairs are created, as previously reported for other alkali-earth molybdates [27]. In KTb, energy transfer from charge carriers to Tb^{3+} luminescence centres appears relatively inefficient, which is evidenced by the presence of only a weak shoulder near 6 eV (Fig. 7c). The intensity of this feature is nearly an order of magnitude lower than that of the main excitonic excitation band. In contrast, K5Tb exhibits much stronger broad excitation bands centred near 5.6 and 6.4 eV, whose intensities decrease only slightly relative to the excitonic band. These observations indicate considerably more efficient energy transfer from free carriers to the Tb^{3+} $^5D_4$ emitting states in the partially disordered lattice. Since such energy-transfer processes are commonly mediated by self-trapped excitons (STEs), structural disorder increases the probability of STE formation and thereby enhances the efficiency of energy transfer to Tb^{3+} centres.

In contrast to potassium terbium double molybdates, the excitation spectra of K5Nd and KNd5 demonstrate a pronounced decrease in intensity in the region of separated e–h pairs creation. This result also confirms the conclusion that despite their different crystal structures, these crystals are characterized by a similar rate of structural disorder.

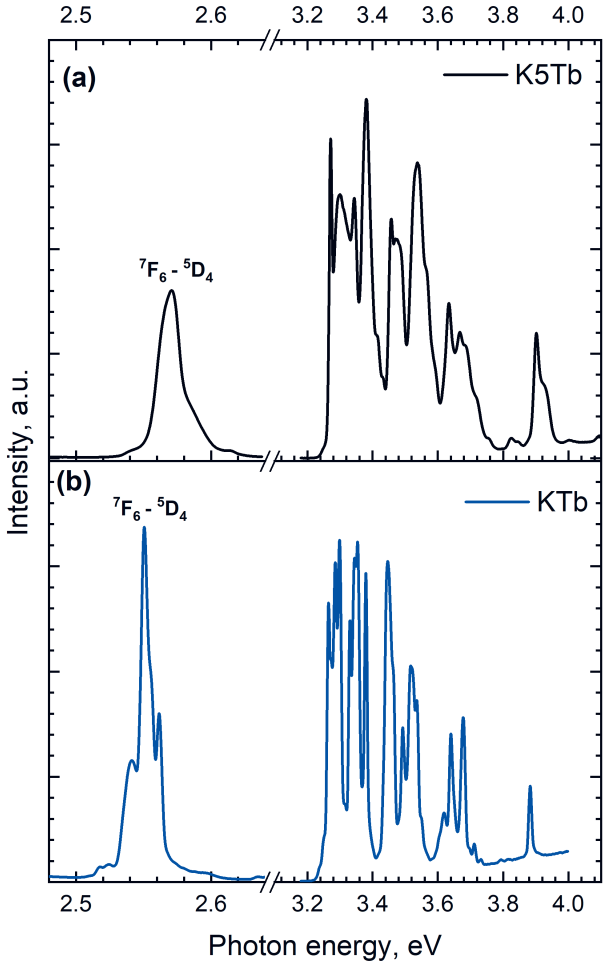

Figure 8: Photoluminescence excitation spectra of K5Tb (a) and KTb (b) measured with spectral resolution 0.4 nm, λ_{em}=545 nm.

At higher excitation energies, approximately corresponding to $2E_g$, an increase in emission intensity was observed for all studied crystals. This enhancement is associated with the multiplication of electronic excitations (MEE) process, in which a single high-energy photon generates multiple electronic excitations. In addition to this conventional MEE process, Tb^{3+} based crystals exhibited another type of MEE effect, regarded as a solid-state analogue of the Frank–Hertz effect. Under interband excitation, the onset of blue emission originating from the Tb^{3+} $^5D_3$ state was observed below the main MEE threshold, indicating that resonant

excitation of Tb^{3+} luminescence centres occurs through impact interaction between hot conduction electrons and Tb^{3+} ions. The experimentally observed threshold energies for the impact excitation of the blue emission agree well with the sum of the fundamental absorption edge energy and the excitation energy of the Tb^{3+} $^5D_3$ level in both KTb and K5Tb crystals.

4.2.3. Luminescence decay kinetics

Luminescence decay kinetics measurements of the studied crystals provide information about the lifetimes of the emitting states and give insight into the radiative and non-radiative relaxation processes governing their emission behaviour. The investigated compounds, belonging to the $K_5RE(MoO_4)_4$ structural type, exhibited decay times typical of the dominant emission of the respective RE^{3+} ions in other compounds. In particular, K5Eu shows red emission at 618 nm originating from the Eu^{3+} $^5D_0$–$^7F_2$ transition, with a decay time of 1.420 ms. Similarly, K5Tb exhibits green emission at 545 nm from the Tb^{3+} $^5D_4$ level, with a decay time of 1.583 ms, while K5Nd shows near-infrared emission at 1065 nm corresponding to the Nd^{3+} $^4F_{3/2}$–$^4I_{11/2}$ transition, with a decay time of 92 μs.

The change of the crystal structure type of the compound formed by the same elements strongly influences the decay time. Significantly shorter decay times are observed in KTb (593 μs) and KNd5 (6.65 μs) than those in K5Tb and K5Nd, respectively. This shortening of the decay time is associated with luminescence quenching caused by the higher concentration of RE^{3+} ions in these compounds. In these structures, the shorter RE-RE ion separation (approximately 4 Å compared to ~6 Å in the K5RE compounds) facilitates energy transfer between neighbouring rare-earth ions and promotes concentration quenching. The quenching process is primarily governed by non-radiative mechanisms such as cross-relaxation and Förster resonance energy transfer (FRET), both of which become increasingly efficient at shorter interionic distances.

In addition, a characteristic cascade relaxation mechanism within the RE^{3+} 4f electronic states is observed in all studied crystals except KNd5, manifested as rise components in the luminescence decay profiles. To illustrate this behaviour, the decay kinetics of K5Eu are discussed as a representative example (Fig. 9). The decay curve of the 618 nm emission was measured at 80 K under 395 nm (3.1 eV) excitation, corresponding to the $^7F_0$–$^5L_6$ absorption transition. As shown in the inset of Fig. 9a, the decay profile exhibits a rise component followed by a single-exponential decay. Fitting with a two-exponential function yields arise time of 11.0 μs and a decay time of 1.420 ms. This rise time matched the decay time of the 535 nm emission originating from the Eu^{3+} $^5D_1$ level (11.00 μs, Fig. 9b), indicating that the population of the $^5D_0$ emitting state is primarily governed by non-radiative relaxation from the higher-lying $^5D_1$ state. Furthermore, an additional rise component of 0.550 μs is observed in the $^5D_1$ emission decay curve, which corresponds to feeding from the $^5D_2$ level. This assignment is supported by independent decay measurements of the $^5D_2$ emission (Fig. 9c), which exhibit two decay components of 0.40 μs and 1.12 μs, yielding an effective

rise time of approximately 0.55 μs for the $^5D_1$ emission. These results collectively confirm a stepwise, cascade-type relaxation process within the Eu^{3+} excited-state manifold, in which higher-lying 4f levels relax non-radiatively to lower states, ultimately populating the emitting $^5D_0$ level responsible for the observed red luminescence at 618 nm.

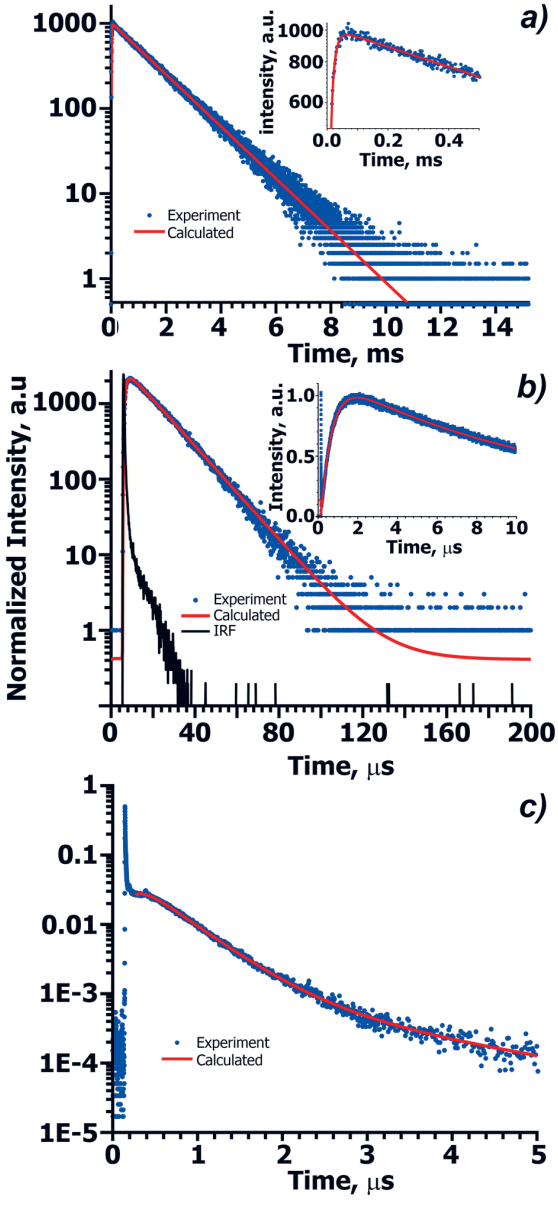

Figure 9. Decay curves of $K_5Eu(MoO_4)_4$ emission measured for radiative transitions from $^5D_0$ (λ_{em} = 618 nm) (a), $^5D_1$ (λ_{em} = 535 nm) (b) and $^5D_2$ (λ_{em} = 486 nm) (c) excited states of Eu^{3+}, E_{ex} = 3.14 eV, T = 80 K for $^5D_0$ and $^5D_1$, and RT for $^5D_2$. In the inset: initial part of the decay, measured with 3-ns pulses of an OPO laser at E_{ex} = 3.14 eV.

A similar cascade relaxation mechanism has been observed in K5Tb, KTb, and K5Nd. In Tb based crystals, the electrons relax from the $^5D_3$ to $^5D_4$ state of Tb^{3+} ions. Similarly, in K5Nd, the relaxation undergoes from the $^4D_{3/2}$ to $^4F_{3/2}$ state of Nd^{3+} ions. However, such processes are not clearly resolved in KNd5 due to the extremely short luminescence lifetime (less than 1 ns) of the higher-lying excited state from which electrons non-radiatively relax to the lowest excited state.

4.2.4. Influence of temperature on luminescence of the double molybdates

Temperature-dependent luminescence studies were conducted to investigate thermal stability of RE^{3+} luminescence in double molybdates and to clarify how it is affected by the variation of crystal structure and excitation energy. Significant differences in the emission quenching temperature (T_q) were observed in the $K_5RE(MoO_4)_4$ system containing Eu^{3+}, Tb^{3+} or Nd^{3+}, where T_q is defined as the temperature at which emission intensity decreases by a factor of two. These differences arise from different electronic configurations of the rare-earth ions, which result in different 4f energy-level structures and varying strengths of electron-phonon interaction. Consequently, the thermal stability of emission varies considerably across the studied systems. Among the investigated compounds, K5Eu exhibits the highest thermal stability, showing the quenching temperature T_q = 564 K for the 618 nm emission under excitation from the ground $^7F_0$ level to the $^5D_2$ level at 2.66 eV (Fig. 10). In comparison, K5Tb shows T_q = 380 K for the $^7F_6$–$^5D_4$ transition (Fig. 11a, left panel), while K5Nd exhibits a significantly lower value of T_q = 200 K for the $^4F_{3/2}$–$^4I_{9/2}$ transition [28]. In addition, both K5Eu and K5Tb systems showed a systematic decrease in quenching temperature with increasing excitation energy.

In K5Eu, T_q decreases from 564 K for the $^7F_0$–$^5D_2$ transition at 2.66 eV to 475 K for the $^7F_0$–$^5L_6$ transition at 3.14 eV, and further to 434 K for the $^7F_0$–$^5D_4$ transition at 3.41 eV (Fig. 10). For the higher-energy $^7F_0$–^5H_J transition at 3.87 eV, the onset of thermal quenching occurred below the low-temperature limit of our setup, and the temperature dependence became similar to that observed under excitation in the fundamental absorption region. The excitation at 5 eV (Fig. 10) corresponds to the creation energy of excitons possessing low thermal stability in K5Eu. A similar trend is observed for the green emission of K5Tb, where T_q decreases from 380 K for the $^7F_6$–$^5D_4$ transitions to 330 K for $^7F_6$–$^5D_3$, $^5G_6$ and further to 267 K for the $^7F_6$–$^5D_0$ transitions (Fig. 11a, b, and c1(left panel). Under interband excitation, T_q decreases to approximately 120 K (Fig. 11 c2), indicating inefficient exciton-mediated energy transfer at elevated temperatures, as also observed for K5Eu.

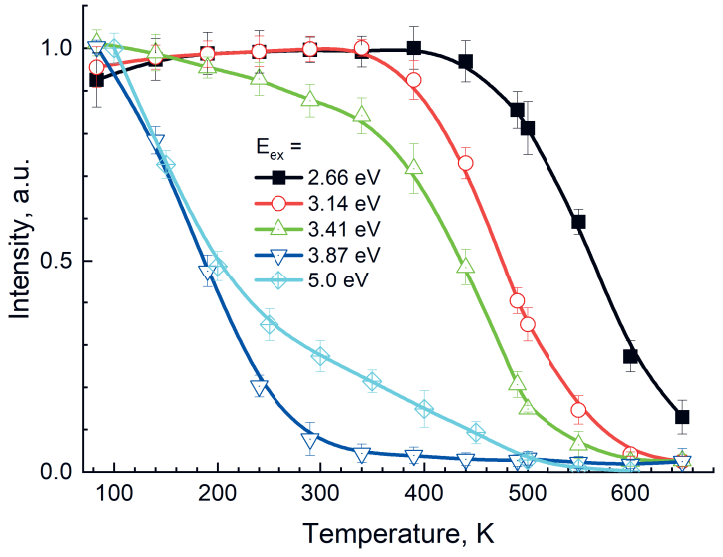

Figure 10: Temperature dependences of the Eu^{3+} emission (λ_{em}=620 nm) in K5Eu for intracentre (E_{ex}= 2.66, 3.14, 3.41, and 3.87 eV) and interband (E_{ex}= 5 eV) transitions from the $^7F_0$ ground state of Eu^{3+}.

The observed shift in T_q with excitation energy in K5Eu and K5Tb can be attributed to the overlap between the RE^{3+} 4f-4f absorption lines and the Urbach tail of the fundamental absorption edge. The Urbach tail shifts to lower energies with increasing temperature due to enhanced electron-phonon interaction, leading to a temperature-dependent increase in absorption in the relevant spectral region. The absorption coefficient in the Urbach tail can reach 10^5–10^6 cm^{-1}, which is two to three orders of magnitude higher than that of parity-forbidden 4f-4f transitions. As this overlap increases, excitation is progressively dominated by interband transitions and exciton formation. However, due to relatively low thermal stability of excitons transferring their energy to RE^{3+} ions, this results in enhanced thermal quenching of RE^{3+} emission.

In contrast, K5Nd exhibits nearly identical temperature dependences under intracentre excitation at 3.5 eV and direct exciton creation at 4.5 eV. This indicates highly efficient, temperature-independent energy transfer from excitons to Nd^{3+} centres up to at least 120 K. The similarity of these dependences suggests strong exciton localization and relatively high thermal stability of excitons in the Nd based system.

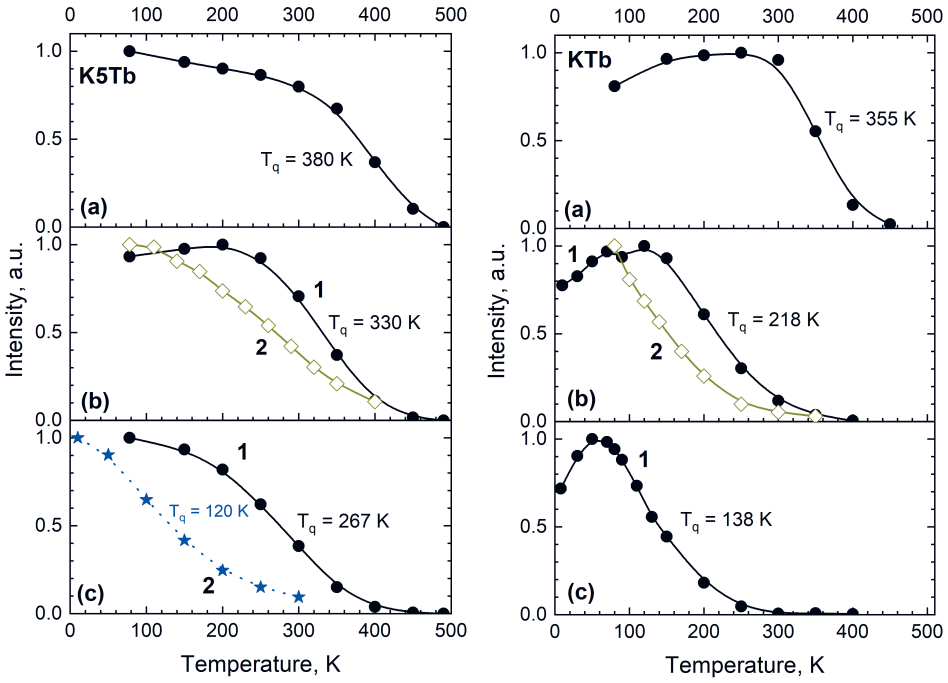

Figure 11. Temperature dependences of the Tb^{3+} 545-nm emission intensity for the transitions $^7F_6$–$^5D_4$ (a), $^7F_6$–$^5D_3$ (b), $^7F_6$–$^5D_0$ (c1), and interband transitions (4.86 eV, c2) in K5Tb (left panel) and KTb (right panel). Curves b2 represent the temperature dependence of the Tb^{3+} 438 nm emission intensity under the $^7F_6$–$^5D_3$ transition (3.28 eV) excitation energy.

The influence of crystal structure on thermal stability of luminescence was analysed by comparing K5Tb with KTb and K5Nd with KNd5. In the Tb-based system, pronounced differences in thermal stability were observed. In KTb, the 545 nm emission excited in the region of the $^7F_6$–$^5D_4$ transition has a lower T_q of approximately 355 K, compared to 380 K observed in K5Tb. For the higher-energy excitations corresponding to the $^7F_6$–$^5D_3$, $^5G_6$, and $^7F_6$–$5D_0$ transitions, T_q decreases further to about 218 K and 138 K, respectively, these values also being lower than in K5Tb showing T_q equal to 330 K and 267 K for these transitions. These differences are primarily due to different band-gap energies in KTb and K5Tb. The narrower band gap in KTb leads to the overlap between the Tb^{3+} 4f states and the Urbach tail of the absorption edge at lower temperatures. Consequently, thermal quenching occurs at lower temperatures in KTb. Additionally, thermal ionization processes may contribute, as higher excited 4f states lie closer to the conduction band.

A similar distinction is observed in the blue emission at 438 nm related to the $^5D_3$–$^7F_4$ transition. In KTb, no clear thermal stability plateau is observed even at 80 K, indicating an early onset of the luminescence quenching. In contrast, K5Tb showed higher luminescence thermal stability with T_q=265 K. This difference is explained by the higher energy position of the conduction band in K5Tb, which delayed overlap with Tb^{3+} excited states.

In contrast, a negligible effect of crystal structure on the thermal stability of NIR luminescence was observed in the Nd^{3+} based systems. Temperature-dependent emission measurements performed under both intracentre (E_{exc} = 3.5 eV) and inter-band excitation (E_{exc} = 4.5 eV) revealed a comparable decrease in emission intensity with increasing temperature for both K5Nd and KNd. These results indicate that the thermal quenching mechanisms are similar in both compounds [28].

SUMMARY

This work is devoted to the investigation of the influence of elemental and structural modifications including structural disorder in potassium rare earth double molybdates on the electronic band structure, energy transfer efficiency to the emission centres and their luminescence characteristics. A set of single crystals of $K_5Eu(MoO_4)_4$, $K_5Tb(MoO_4)_4$, $KTb(MoO_4)_2$, $K_5Nd(MoO_4)_4$, and $KNd_5(MoO_4)_8$ were studied using a variety of experimental methods including time-resolved photoluminescence spectroscopy using synchrotron radiation with the focus placed on the dependence of energy transfer processes to RE^{3+} emission centres on temperature. The performed study highlights the importance of crystal structure type and ordering in determining the photoluminescence characteristics of RE^{3+} ions and its thermal stability in double molybdates.

The main conclusions are the following:

1. The emission typical of the intra-configurational 4f–4f transitions in RE^{3+} ions was observed in luminescence spectra. The substitution of RE^{3+} ions enables emission colour tuning in a broad spectral range, with Tb^{3+} producing intense green emission 480–640 nm corresponding to the $^5D_4$–^7F_J transitions, Eu^{3+} exhibiting red emission in the 520–720 nm region due to the $^5D_0$–^7F_J transitions, and Nd^{3+} emitting in the near-infrared region at 850–950 nm due to the $^4F_{3/2}$–$^4I_{9/2}$, $^4I_{11/2}$ transitions.
2. For the first time intrinsic emission of self-trapped excitons was detected in double potassium molybdates $K_5Nd(MoO_4)_4$, and $KNd_5(MoO_4)_8$. An unusually short lifetime of the STE emission in the nanosecond range and its low intensity are ascribed to a rapid energy transfer from the STEs to the Nd^{3+} ions.
3. It is shown that the crystal structure exerts a profound influence on the luminescence characteristics. The incommensurately modulated $K_5Tb(MoO_4)_4$ crystal exhibited a broader and more intense green emission than the ordered $KTb(MoO_4)_2$ crystal, which is ascribed to the availability of multiple non-equivalent sites in the lattice and the effect of partial structural disorder of crystal structure of $K_5Tb(MoO_4)_4$. The luminescence intensity enhancement in $K_5Tb(MoO_4)_4$ is attributed to the structural disorder induced suppression of concentration quenching, as a result of the hindering of nonradiative energy transfer between neighbouring Tb^{3+} ions.
4. The studies of the reflectivity and excitation spectra indicated a negligible contribution of the electronic states of potassium and rare-earth ions to the formation of the valence band and the bottom of the conduction band in the investigated compounds. In particular, the analysis of reflection spectra of $K_5Nd(MoO_4)_4$ and $KNd_5(MoO_4)_8$ demonstrated that the main features observed in the fundamental absorption region can be attributed to the electronic transitions from the 2p O states forming the valence band to the 4d Mo states of the conduction band. The contribution of potassium electronic states is

shown to be remarkable for $K_5Nd(MoO_4)_4$ in the region 18–28 eV, which is ascribed to the electron transitions from the 3p K core states to high-density states in the conduction band as well as to the formation of core excitons with a hole component localized at the 3p K states.

5. The analysis of the excitation spectra in the fundamental absorption region allowed to clarify the peculiarities of the energy transfer from separated electrons and holes to RE^{3+} ions. The absence of the UV charge-transfer band in $K_5Eu(MoO_4)_4$ and inter-valence charge-transfer band below the fundamental absorption edge of $K_5Tb(MoO_4)_4$ and $KTb(MoO_4)_2$ indicated that the ground 4f levels of RE^{3+} are located within or near the valence band in double molybdates. It is concluded that energy transfer from separated electrons and holes in the conduction and valence bands, respectively, is realized via an intermediate self-trapped exciton state.

6. The efficiency of the energy transfer from separated electrons and holes to RE^{3+} emission centres is shown to depend on the disorder rate of the crystal structure. It is established that the structural disorder promotes exciton formation by decreasing the mean free path length of charge carriers during the migration stage.

7. For $K_5Tb(MoO_4)_4$ and $KTb(MoO_4)_2$ crystals, different mechanisms are proposed for energy transfer to the excited $^5D_4$ and $^5D_3$ terms, which are responsible for the green and blue sets of emission lines. The energy transfer from STEs to Tb^{3+} is realized via the excitation of the lowest excited term $^5D_4$, giving rise only to the green emission. The term $^5D_3$ responsible for the blue emission can be excited either via the intra-centre excitation of Tb^{3+} or via the resonant excitation of the Tb^{3+} ions through the inelastic relaxation of hot electrons in the conduction band (so called solid-state analogue of the Frank-Hertz effect).

8. It is established that the thermal stability of the RE^{3+} emission depends strongly on excitation energy. In the Eu^{3+} and Tb^{3+} based systems, the quenching temperature decreases with increasing excitation energy due to the enhanced overlap of the RE^{3+} 4f excited states with the temperature-dependent Urbach tail of the fundamental absorption edge. Under the interband excitation above the fundamental absorption edge, thermal quenching occurs at significantly lower temperatures determined by the stability of the STE state. Crystal structure variation significantly influenced the luminescence thermal stability in Tb-based double molybdates, with the bandgap varying with structure, thereby defining the rate of thermal ionization of the emission centre. In general, the variation of thermal stability of the emission with the excitation energy is attractive for the application of these crystals in non-contact luminescence thermometry.

9. The decay kinetics measurements showed that the $K_5RE(MoO_4)_4$ compounds exhibit long luminescence lifetimes ranging from milliseconds for $K_5Eu(MoO_4)_4$, and $K_5Tb(MoO_4)_4$ to hundred microseconds for $K_5Nd(MoO_4)_4$. In contrast, $KTb(MoO_4)_2$ and $KNd_5(MoO_4)_8$ show significantly shorter decay times due to concentration quenching arising from the reduced RE-RE distances and enhanced nonradiative cross-relaxation and Förster resonance energy transfer. A cascade type relaxation between various excited states of RE^{3+} is observed in all investigated double molybdates, except $KNd_5(MoO_4)_8$, in which this relaxation is too fast to be resolved by the experimental setups used.

KOKKUVÕTE

Energia ülekanne kiirgustsentrile leelismetallide ja haruldaste muldmetallide molübdaatides

Doktoritöö on pühendatud elementkoostise ja struktuursete muutuste, sealhulgas struktuurse korratuse, mõju uurimisele kaaliumi ja haruldaste muldmetallide topeltmolübdaatide elektroonse tsoonstruktuurile, energia ülekande efektiivsusele kiirgustsentritele ning luminestsentsi omadustele. Uuriti $K_5Eu(MoO_4)_4$, $K_5Tb(MoO_4)_4$, $KTb(MoO_4)_2$, $K_5Nd(MoO_4)_4$, ja $KNd_5(MoO_4)_8$ monokristalle, kasutades erinevaid eksperimentaalseid meetodeid, sealhulgas aeglahutusega fotoluminestsents-spektroskoopiat kasutades sünkrotronkiirgust ning pöörates erilist tähelepanu RE^{3+} kiirgustsentrile energia ülekande protsesside temperatuurisõltuvusele. Läbiviidud uuring rõhutab kristallstruktuuri tüübi ja korrastatuse olulist rolli haruldaste muldmetallide ioonide fotoluminestsentsi omaduste ning selle termilise stabiilsuse määramisel topeltmolübdaatides.

Peamised järeldused on järgmised:

1. Luminestsentsspektrites täheldati RE^{3+} ioonide iseloomulikke 4f–4f sisekonfiguratsioonilistele üleminekutele vastavaid kiirguseid. RE^{3+} ioonide asendamine võimaldab kiirguse värvi häälestamist laias spektraalses vahemikus: Tb^{3+} tekitab intensiivset rohelist kiirgust 480–640 nm vahemikus, mis vastab üleminekutele $^5D_4$–^7F_J; Eu^{3+} kiirgab punases piirkonnas 520–720 nm $^5D_0$–^7F_J üleminekute tõttu; Nd^{3+} kiirgab lähisinfrapunases piirkonnas 850–950 nm, mis vastab $^4F_{3/2}$–$^4I_{9/2}$ ja $^4I_{11/2}$ üleminekutele.

2. Esmakordselt tuvastati topeltmolübdaatides $K_5Nd(MoO_4)_4$ ja $KNd_5(MoO_4)_8$ iselõksustunud eksitonidega seotud omakiirgus. Seda kiirgust iseloomustab ebatavaliselt lühike eluiga nanosekundite ajavahemikus, ning selle madal intensiivsus seostati kiire energia ülekandega eksitonidelt Nd^{3+} ioonidele.

3. Näidati, et kristallstruktuur mõjutab oluliselt luminestsentsi omadusi. Kõrglahutusega ergastusspektrite analüüs näitas, et Eu^{3+} ioonid asuvad $K_5Eu(MoO_4)_4$-s vähemalt kolmes mitteekvivalentses kristallograafilises positsioonis, mis on seotud selle kristalli moduleeritud superstruktuuriga. Superstruktuurselt moduleeritud $K_5Tb(MoO_4)_4$ kristallil on laiem ja intensiivsem roheline kiirgusriba võrreldes korrastatud $KTb(MoO_4)_2$ kristalliga, mida seostatakse mitmete mitteekvivalentsete Tb^{3+} sõlmede olemasoluga võres ning osalise struktuurse korratuse mõjuga. Luminestsentsi intensiivsuse suurenemine $K_5Tb(MoO_4)_4$-s on seotud struktuursest korratusest tingitud kontsentratsioonilise kustumise pärssimisega läbi mittekiirguslikku energiaülekande takistamise lähedal asuvate Tb^{3+} ioonide vahel.

4. Elektroonilise tsoonstruktuuri uuringud näitasid, et kaaliumi ja haruldaste muldmetallide ioonide elektroonsetel olekutel on uuritud $K_5RE(MoO_4)_4$ ühendites tühine mõju valents- ja juhtivustsoonide kujunemisele. Eelkõige näitas

$K_5Nd(MoO_4)_4$ ja $KNd_5(MoO_4)_8$ peegeldusspektrite analüüs, et põhilised tunnused, mis on jälgitavad fundamentaalneeldumise piirkonnas, tulenevad üleminekutest 2p O seisunditelt valentstsoonis 4d Mo seisunditele juhtivustsoonis. Kaaliumi elektroonsete olekute panus on oluline 18–28 eV piirkonnas, mida seostatakse üleminekutega 3p K sisekihilt juhtivustsooni kõrge tihedusega elektronseisunditele ning süvakihieksitoni tekkega, mille augukomponent on lokaliseerunud 3p K seisundis.

5. Ergastusspektrite analüüs fundamentaalneeldumispiirkonnas võimaldas selgitada välja energia ülekande iseärasusi eraldatud elektronidelt ja aukudelt RE^{3+} ioonidele. Laenguülekande UV riba puudumine $K_5Eu(MoO_4)_4$ kristallis ning intervalentse laenguülekande riba puudumine $K_5Tb(MoO_4)_4$ ja $KTb(MoO_4)_2$ puhul fundamentaalneeldumise ääre all näitab, et RE^{3+} ioonide 4f põhiseisundid asuvad topeltmolübdaatides valentstsooni sees. Järeldatakse, et energia ülekanne eraldatud elektronidelt ja aukudelt toimub vahepealse iselõksustunud eksitoni seisundi kaudu.

6. Näidati, et energia ülekande efektiivsus eraldatud elektronidelt ja aukudelt RE^{3+} kiirgustsentrile sõltub kristallstruktuuri korratuse määrast. Leiti, et struktuurne korratus soodustab eksitonide teket, vähendades laengukandjate keskmist vabatee pikkust migratsioonifaasis.

7. $K_5Tb(MoO_4)_4$ ja $KTb(MoO_4)_2$ kristallide puhul pakuti välja erinevaid energia ülekande mehhanisme ergastatud $^5D_4$ ja $^5D_3$ nivoodele, mis vastutavad rohelise ja sinise kiirguse eest. Energiaülekanne iselõksustunud eksitonidelt Tb^{3+} ioonidele toimub madalaimale $^5D_4$ ergastatud seisundile, mis annab ainult rohelist kiirgust. $^5D_3$ seisund, mis vastutab sinise kiirguse eest, võib ergastuda kas Tb^{3+} tsentrisisese ergastuse kaudu või resonantse ergastuse kaudu juhtivustsooni kuumade elektronide mitteelastse relaksatsiooni käigus (nn Frank–Hertzi efekti tahkisanaloog).

8. Leiti, et RE^{3+} kiirguse termiline stabiilsuse määrab tugevalt nii haruldaste muldmetallide asendamine kui ka ergastuse energia. $K_5RE(MoO_4)_4$ ühendite seas näitab $K_5Eu(MoO_4)_4$ kõrgeimat termilise kustumise temperatuuri T_q, millele järgnevad $K_5Tb(MoO_4)_4$ ja $K_5Nd(MoO_4)_4$. Eu^{3+} ja Tb^{3+} süsteemides väheneb T_q samuti ergastuse energia suurenedes, kuna RE^{3+} 4f ergastatud seisundite kattuvus temperatuurist sõltuva Urbachi sabaga fundamentaalneeldumise ääre lähedal suureneb. Tsoonidevahelise ergastuse korral fundamentaalneeldumise äärest kõrgemal toimub termiline kustumine oluliselt madalamatel temperatuuridel, mille määrab eksitonseisundi madal stabiilsus. Kristallstruktuuri varieerumine mõjutas oluliselt kiirguse termilist stabiilsust terbiumil põhinevates topeltmolübdaatides, kus keelutsooni laius sõltub kristallstruktuurist, mis määrab kiirgustsentri termilise ionisatsiooni kiiruse. Üldiselt on kiirguse termilise stabiilsuse sõltuvus ergastuse energiast atraktiivne nende kristallide kasutamiseks kontaktivabas luminestsents-termomeetrias.

9. Kiirguse kustumiskineetika mõõtmised näitasid, et $K_5RE(MoO_4)_4$ ühenditel on luminestsentsi eluajad pikad, ulatudes millisekunditest $K_5Eu(MoO_4)_4$ ja $K_5Tb(MoO_4)_4$ puhul kuni sadade mikrosekunditeni $K_5Nd(MoO_4)_4$ puhul. Seevastu $KTb(MoO_4)_2$ ja $KNd_5(MoO_4)_8$ näitavad oluliselt lühemaid kustumisaegu, mis on tingitud kontsentratsioonilisest kustumisest, mis on tingitud väiksematest RE-RE kaugustest ning vastavalt efektiivsemast mittekiirguslikust ristrelaksatsioonist ja Försteri resonantsest energiaülekandest. Kaskaadrelaksatsiooni erinevate ergastatud RE^{3+} seisundite vahel täheldati kõigis uuritud topeltmolübdaatides, välja arvatud KNd5$(MoO_4)_8$, kus see relaksatsioon on liiga kiire, et selle aega kasutatud eksperimentaalse seadmete abil määrata.

ACKNOWLEDGEMENTS

I would like to express my sincere gratitude to my supervisors, Dr. Vitali Nagirnyi and Dr. Dmitry Spassky, for their continuous support, guidance, and encouragement throughout my doctoral studies and the preparation of this thesis. I am also grateful to the Head of the Laboratory of Physics of Ionic Crystals, Prof. Aleksandr Lushchik, for providing the opportunity to conduct my research in this laboratory.

I sincerely thank Prof. Marco Kirm, Dr. Eduard Feldbach, and Dr. Ivo Romet for their expertise in spectroscopy and valuable technical assistance during the experimental work. My gratitude is extended to B. Redkin and V. A. Morozov for providing the crystals studied in this work, as well as to Dr. Hugo Mändar for X-ray diffraction (XRD) analysis and to Mr. Peeter Ritslaid for X-ray fluorescence (XRF) measurements from the Laboratory of Thin Films. I also acknowledge Dr. Kirill Chernenko for his support during experiments at the FinEstBeAMS beamline (MAX IV Laboratory, Lund) and Dr. Aleksei Kotlov and Dr. Yevheniia Smortsova for their assistance at the P66 beamline at DESY. I am also thankful to all members of the Laboratory of Physics of Ionic Crystals for their collegial atmosphere, support, and discussions throughout my studies.

Finally, I express my deepest gratitude to my family and friends for their unwavering support and encouragement during my academic journey.

This work has been supported by Estonian Research Council grant PRG2733, the ERDF funding in Estonia granted to the Centre of Excellence TK210 “Centre of Excellence in Sustainable Green Hydrogen and Energy Technologies” and TWINNING project “EXANST” funded by the European Union under grant agreement No. 101159716.

REFERENCES

[1] S.M. Posokhova, V.A. Morozov, D.V. Deyneko, B.S. Redkin, D.A. Spassky, V. Nagirnyi, A.A. Belik, J. Hadermann, E.T. Pavlova, B.I. Lazoryak, $K_5Eu(MoO_4)_4$ red phosphor for solid state lighting applications, prepared by different techniques, CrystEngComm 25 (2023) 835–847. https://doi.org/10.1039/D2CE01107G.

[2] L. Yi, L. Zhou, Z. Wang, J. Sun, F. Gong, W. Wan, W. Wang, $KGd(MoO_4)_2:Eu^{3+}$ as a promising red phosphor for light-emitting diode application, Current Applied Physics 10 (2010) 208–213. https://doi.org/10.1016/j.cap.2009.05.025.

[3] Z.Q. Wu, J.F. Tang, J.H. Huang, X.H. Gong, Y.J. Chen, Y.F. Lin, Z.D. Luo, Y.D. Huang, Polarized spectral properties of $Tm^{3+}:K_5Bi(MoO_4)_4$ crystal, Optical Materials 34 (2011) 287–291. https://doi.org/10.1016/j.optmat.2011.08.032.

[4] P. Armand, C. Reibel, D. Granier, M. Tillard, Growth, single-crystal structure, and magnetic properties of the double molybdate $KYb(MoO_4)_2$, Journal of Physics and Chemistry of Solids 154 (2021) 110023. https://doi.org/10.1016/j.jpcs.2021.110023.

[5] M. Voda, I. Iparraguire, J. Fernández, R. Balda, M. Al-Saleh, A. Mendioroz, G. Lobera, M. Cano, M. Sanz, J. Azkargorta, Laser properties of Nd^{3+} in $K_5Nd(MoO_4)_4$ stoichiometric disordered crystal, Optical Materials 16 (2001) 227–231. https://doi.org/10.1016/S0925-3467(00)00082-3.

[6] A. Li, D. Xu, H. Lin, S. Yang, Y. Shao, Y. Zhang, $NaGd(MoO_4)_2$ nanocrystals with diverse morphologies: controlled synthesis, growth mechanism, photoluminescence and thermometric properties, Sci Rep 6 (2016) 31366. https://doi.org/10.1038/srep31366.

[7] Z. Chen, A. Khan, X. Wang, J. Zhang, S. Pan, H. Kim, J. Pan, Low temperature luminescence and scintillation properties of $NaLa(MoO_4)_2$ crystal grown by the vertical Bridgman method, Journal of Luminescence 231 (2021) 117780. https://doi.org/10.1016/j.jlumin.2020.117780.

[8] A.A. Kaminskii, S.E. Sarkisov, J. Bohm, P. Reiche, D. Schultze, R. Uecker, Growth, spectroscopic and laser properties of crystals in the $K_5Bi_{1-x}Nd_x(MoO_4)_4$ system, Phys. Stat. Sol. (a) 43 (1977) 71–79. https://doi.org/10.1002/pssa.2210430106.

[9] V.A. Morozov, S.M. Posokhova, S.Ya. Istomin, D.V. Deyneko, A.A. Savina, B.S. Redkin, N.V. Lyskov, D.A. Spassky, A.A. Belik, B.I. Lazoryak, $KTb(MoO_4)_2$ Green Phosphor with K^+ -Ion Conductivity: Derived from Different Synthesis Routes, Inorg. Chem. 60 (2021) 9471–9483. https://doi.org/10.1021/acs.inorgchem.1c00597.

[10] M. Dan, C. Niu, Y. Yu, X. Zhu, W. Zhang, H. Ye, Z. Li, Y. Wang, K.R. Poeppelmeier, Regulation of color tunability of Dy^{3+}/Eu^{3+} -based double molybdate phosphors with high thermal stability, New J. Chem. 49 (2025) 5352–5361. https://doi.org/10.1039/D5NJ00044K.

[11] S.M. Posokhova, V.A. Morozov, D.V. Deyneko, I.V. Nikiforov, B.S. Redkin, D.A. Spassky, A.A. Belik, E.T. Pavlova, B.I. Lazoryak, $K_5Eu_{1-x}Tb_x(MoO_4)_4$ Phosphors for Solid-State Lighting Applications: Aperiodic Structures and the $Tb^{3+} \rightarrow Eu^{3+}$ Energy Transfer, Inorg. Chem. 61 (2022) 7910–7921. https://doi.org/10.1021/acs.inorgchem.2c00548.

[12] M. Piasecki, E. Mandowska, A. Herrmann, D. Ehrt, A. Majchrowski, L.R. Jaroszewicz, M.G. Brik, I.V. Kityk, Tailoring Nd3+ luminescence characteristics by Yb^{3+} doping in $K_5Nd(MoO_4)_4$, $RbNd(WO_4)_2$ and $NdAl_3(BO_3)_4$ crystal matrices, Journal of Alloys and Compounds 639 (2015) 577–582. https://doi.org/10.1016/j.jallcom.2015.03.018.

[13] G. Benoît, J. Véronique, A. Arnaud, G. Alain, Luminescence properties of tungstates and molybdates phosphors: Illustration on $ALn(MO_4)_2$ compounds (A = alikaline cation, Ln = lanthanides, M = W, Mo), Solid State Sciences 13 (2011) 460–467. https://doi.org/10.1016/j.solidstatesciences.2010.12.013.

[14] V.A. Morozov, S.M. Posokhova, D.V. Deyneko, A.A. Savina, A.V. Morozov, O.A. Tyablikov, B.S. Redkin, D.A. Spassky, J. Hadermann, B.I. Lazoryak, Influence of annealing conditions on the structure and luminescence properties of $KGd_{1-x}Eu_x(MoO_4)_2$ ($0 \leq x \leq 1$), CrystEngComm 21 (2019) 6460–6471. https://doi.org/10.1039/C9CE01244C.

[15] M. Korzhik, G. Tamulaitis, A.N. Vasil'ev, Physics of Fast Processes in Scintillators, Springer International Publishing, Cham, 2020. https://doi.org/10.1007/978-3-030-21966-6.

[16] P. Armand, C. Reibel, D. Granier, M. Tillard, Growth, single-crystal structure, and magnetic properties of the double molybdate $KYb(MoO_4)_2$, Journal of Physics and Chemistry of Solids 154 (2021) 110023. https://doi.org/10.1016/j.jpcs.2021.110023.

[17] B.I. Lazoryak, V.A. Efremov, Structural features of α-$K_5Y(MoO_4)_4$ single crystals, Kristallografiya 26 (1981) 464–472.

[18] B.I. Lazoryak, V.A. Efremov, The structure of palmierite-like $K_5Nd(MoO_4)_4$, $K_5Bi(MoO_4)_4$, $Rb_5Gd(MoO_4)_4$, Kristallografiya 31 (1986) 237–243.

[19] P. Dorenbos, A.H. Krumpel, E. Van Der Kolk, P. Boutinaud, M. Bettinelli, E. Cavalli, Lanthanide level location in transition metal complex compounds, Optical Materials 32 (2010) 1681–1685. https://doi.org/10.1016/j.optmat.2010.02.021.

[20] E.V. Vasil'ev, A.A. Evdokimov, V.A. Efremov, B.I. Lazoryak, V.F. Papulovskii, R.K. Sviridova, A.F. Solokha, V.K. Trunov, The spectral and structural properties of $K_5Nd(MoO_4)_4$, J Appl Spectrosc 29 (1978) 1342–1345. https://doi.org/10.1007/BF00604761.

[21] Y. Smortsova, O. Chukova, M. Kirm, V. Nagirnyi, V. Pankratov, A. Kataev, A. Kotlov, The P66 time-resolved VUV spectroscopy beamline at PETRA III storage ring of DESY, J Synchrotron Rad 32 (2025) 1539–1548. https://doi.org/10.1107/S1600577525007568.

[22] V. Pankratov, R. Pärna, M. Kirm, V. Nagirnyi, E. Nõmmiste, S. Omelkov, S. Vielhauer, K. Chernenko, L. Reisberg, P. Turunen, A. Kivimäki, E. Kukk, M. Valden, M. Huttula, Progress in development of a new luminescence setup at the FinEstBeAMS beamline of the MAX IV laboratory, Radiation Measurements 121 (2019) 91–98. https://doi.org/10.1016/j.radmeas.2018.12.011.

[23] K. Chernenko, A. Kivimäki, R. Pärna, W. Wang, R. Sankari, M. Leandersson, H. Tarawneh, V. Pankratov, M. Kook, E. Kukk, L. Reisberg, S. Urpelainen, T. Käämbre, F. Siewert, G. Gwalt, A. Sokolov, S. Lemke, S. Alimov, J. Knedel, O. Kutz, T. Seliger, M. Valden, M. Hirsimäki, M. Kirm, M. Huttula, Performance and characterization of the FinEstBeAMS beamline at the MAX IV Laboratory, J Synchrotron Rad 28 (2021) 1620–1630. https://doi.org/10.1107/S1600577521006032.

[24] Bachmann, H. G, Kleber, W, Die struktur des palmierits und ihre isotypie-beziehungen, Fortschr. Mineral 31 (1952) 9–11.

[25] Chr.K. Møller, P. Yum, H. Zachariasen, A.I. Virtanen, The Structure of $Pb(NH_4)_2(SO_4)_2$ and Related Compounds., Acta Chem. Scand. 8 (1954) 81–87. https://doi.org/10.3891/acta.chem.scand.08-0081.

[26] M.U. Jamal, V. Nagirnyi, K. Chernenko, A. Kotlov, Y. Smortsova, D. Spassky, Crystal structure controlled energy transfer to Tb3+ in $KTb(MoO_4)_2$ and $K_5Tb(MoO_4)_4$ crystals, Materials Research Bulletin 191 (2025) 113553. https://doi.org/10.1016/j.materresbull.2025.113553.
[27] D.A. Spassky, N.S. Kozlova, V. Nagirnyi, A.E. Savon, Yu.A. Hizhnyi, S.G. Nedilko, Excitation energy transfer to luminescence centers in $MIIMoO_4$ (MII=Ca, Sr, Zn, Pb) and Li_2MoO_4, Journal of Luminescence 186 (2017) 229–237. https://doi.org/10.1016/j.jlumin.2017.02.048.
[28] M.U. Jamal, V. Nagirnyi, H. Mändar, K. Chernenko, D. Spassky, Structural and luminescence properties of $K_5Nd(MoO_4)_4$ and $KNd_5(MoO_4)_8$, Journal of Luminescence (2026) 121995. https://doi.org/10.1016/j.jlumin.2026.121995.

PUBLICATIONS

CURRICULUM VITAE

Name: Muhammad Usama Jamal
Date of birth: 27.02.1994
Nationality: Pakistani
Phone number: +372 5787 4061
E-mail: muhammad.usama.jamal@ut.ee
Occupation: Junior research fellow, Laboratory of Physics of Ionic Crystals, Institute of Physics, University of Tartu

Education:

2020–2022	MSc, Materials Science and Technology, University of Tartu, Estonia
2022–2026	PhD, University of Tartu

Languages:

Urdu	Native
English	Good
Estonian	Beginner

Career:

2022–2026	Junior research fellow, Laboratory of Physics of Ionic Crystals, Institute of Physics, University of Tartu, Estonia.

Research interests:

Solid-state physics, crystal growth and materials synthesis, luminescent materials (phosphors and scintillators), and steady-state and time-resolved optical spectroscopy.

Publications:

M.U. Jamal, V. Nagirnyi, H. Mändar, K. Chernenko, D. Spassky, Structural and luminescence properties of $K_5Nd(MoO_4)_4$ and $KNd_5(MoO_4)_8$, Journal of Luminescence (2026) 121995. https://doi.org/10.1016/j.jlumin.2026.121995.

M.U. Jamal, V. Nagirnyi, K. Chernenko, A. Kotlov, Y. Smortsova, D. Spassky, Crystal structure controlled energy transfer to Tb_{3+} in $KTb(MoO_4)_2$ and $K_5Tb(MoO_4)_4$ crystals, Materials Research Bulletin 191 (2025) 113553. https://doi.org/10.1016/j.materresbull.2025.113553.

D. Spassky, A. Vasil'ev, **M.U. Jamal**, V.A. Morozov, B.I. Lazoryak, B.S. Redkin, K. Chernenko, V. Nagirnyi, Temperature dependent energy transfer to Eu^{3+} emission centres in $K_5Eu(MoO_4)_4$ crystals, CrystEngComm 26 (2024) 1106–1116. https://doi.org/10.1039/D3CE01201H.

Conference presentations:

Jamal, Muhammad Usama; Nagirnyi, Vitali; Spassky, Dmitry, "Influence of crystal structure on energy transfer to Tb^{3+} in $K_5Tb(MoO_4)_4$ and $KTb(MoO_4)_2$ crystals", oral presentation at the FMNT & NIBS Conference, October 2024, Tartu, Estonia.

Jamal, Muhammad Usama; Nagirnyi, Vitali; Spassky, Dmitry, "The influence of crystal structure on luminescence properties of Tb^{3+} in double molybdates", poster presentation at the 8th Baltic electrochemistry conference, April 2024.

Jamal, Muhammad Usama; Nagirnyi, Vitali; Spassky, Dmitry, "The impact of crystal structure on Tb^{3+} luminescence in double molybdates", poster presentation at the LUMDETR 2024 Conference, June 2024, Riga, Latvia.

Jamal, Muhammad Usama; Nagirnyi, Vitali; Spassky, Dmitry; "Luminescence properties of $K_5Eu(MoO_4)_4$", poster and 3-minute oral presentation at the GSFMT Scientific Conference, 2023, Tartu, Estonia.

Awards and scholarships:

2024 Received mobility grant from Estonian Doctoral School to visit the LUMDETR 2024 Conference, Riga, Latvia.

2020–2022 Awarded specialization and performance scholarships multiple times during my master's studies.

ELULOOKIRJELDUS

Nimi: Muhammad Usama Jamal
Sünniaeg: 27.02.1994
Kodakondsus: Pakistanlane
Telefon: +372 57874061
E-post: muhammad.usama.jamal@ut.ee
Töökoht, amet: Nooremteadur, Ioonkristallide füüsika labor, Füüsika Instituut, Tartu Ülikool

Haridus:

2020–2022	MSc, materjaliteadus ja tehnoloogia, Tartu Ülikool, Eesti
2022–2026	Doktoriõpe, Tartu Ülikool

Keelteoskus:

Urdu keel	emakeel
Inglise keel	hea
Eesti keel	algtase

Töökogemus:

2022–2026	Nooremteadur, Ioonkristallide füüsika labor, Füüsika Instituut, Tartu Ülikool.

Peamised uurimisvaldkonnad:

Tahkisfüüsika, kristallide kasvatamine ja materjalide süntees, luminestsents-materjalid (fosfoorid ja stsintillaatorid) ning statsionaarne ja ajalise lahutusega optiline spektroskoopia.

Publikatsioonid:

M.U. Jamal, V. Nagirnyi, H. Mändar, K. Chernenko, D. Spassky, Structural and luminescence properties of $K_5Nd(MoO_4)_4$ and $KNd_5(MoO_4)_8$, Journal of Luminescence (2026) 121995. https://doi.org/10.1016/j.jlumin.2026.121995.

M.U. Jamal, V. Nagirnyi, K. Chernenko, A. Kotlov, Y. Smortsova, D. Spassky, Crystal structure controlled energy transfer to Tb_{3+} in $KTb(MoO_4)_2$ and $K_5Tb(MoO_4)_4$ crystals, Materials Research Bulletin 191 (2025) 113553. https://doi.org/10.1016/j.materresbull.2025.113553.

D. Spassky, A. Vasil'ev, **M.U. Jamal**, V.A. Morozov, B.I. Lazoryak, B.S. Redkin, K. Chernenko, V. Nagirnyi, Temperature dependent energy transfer to Eu^{3+} emission centres in $K_5Eu(MoO_4)_4$ crystals, CrystEngComm 26 (2024) 1106–1116. https://doi.org/10.1039/D3CE01201H.

Konverentsiettekanded:

Jamal, Muhammad Usama; Nagirnyi, Vitali; Spassky, Dmitry, "Influence of crystal structure on energy transfer to Tb^{3+} in $K_5Tb(MoO_4)_4$ and $KTb(MoO_4)_2$ crystals", Suuline ettekanne FMNT & NIBS konverentsil, oktoober 2024, Tartu, Eesti.

Jamal, Muhammad Usama; Nagirnyi, Vitali; Spassky, Dmitry, "The influence of crystal structure on luminescence properties of Tb^{3+} in double molybdates", posterettekanne 8. Balti elektrokeemia konverentsil, aprill 2024, Tartu, Eesti.

Jamal, Muhammad Usama; Nagirnyi, Vitali; Spassky, Dmitry, "The impact of crystal structure on Tb^{3+} luminescence in double molybdates", Posterettekanne LUMDETR 2024 konverentsil, juuni 2024, Riia, Läti..

Jamal, Muhammad Usama; Nagirnyi, Vitali; Spassky, Dmitry; "Luminescence properties of $K_5Eu(MoO_4)_4$", Posterettekanne ja 3-minutiline suuline ettekanne GSFMT teaduskonverentsil, 2023, Tartu, Eesti.

Saadud uurimistoetused ja stipendiumid:

2024 Saadud Eesti doktorkooli mobiilsustoetus osalemiseks LUMDETR 2024 konverentsil Riias, Lätis.

2020–2022 Magistriõpingute jooksul mitmel korral eriala- ja tulemusstipendiumide määramine.

DISSERTATIONES PHYSICAE UNIVERSITATIS TARTUENSIS

1. **Andrus Ausmees**. XUV-induced electron emission and electron-phonon interaction in alkali halides. Tartu, 1991.
2. **Heiki Sõnajalg**. Shaping and recalling of light pulses by optical elements based on spectral hole burning. Tartu, 1991.
3. **Sergei Savihhin**. Ultrafast dynamics of F-centers and bound excitons from picosecond spectroscopy data. Tartu, 1991.
4. **Ergo Nõmmiste**. Leelishalogeniidide röntgenelektronemissioon kiiritamisel footonitega energiaga 70–140 eV. Tartu, 1991.
5. **Margus Rätsep**. Spectral gratings and their relaxation in some low-temperature impurity-doped glasses and crystals. Tartu, 1991.
6. **Tõnu Pullerits**. Primary energy transfer in photosynthesis. Model calculations. Tartu, 1991.
7. **Olev Saks**. Attoampri diapasoonis voolude mõõtmise füüsikalised alused. Tartu, 1991.
8. **Andres Virro**. AlGaAsSb/GaSb heterostructure injection lasers. Tartu, 1991.
9. **Hans Korge**. Investigation of negative point discharge in pure nitrogen at atmospheric pressure. Tartu, 1992.
10. **Jüri Maksimov**. Nonlinear generation of laser VUV radiation for high-resolution spectroscopy. Tartu, 1992.
11. **Mark Aizengendler**. Photostimulated transformation of aggregate defects and spectral hole burning in a neutron-irradiated sapphire. Tartu, 1992.
12. **Hele Siimon**. Atomic layer molecular beam epitaxy of A^2B^6 compounds described on the basis of kinetic equations model. Tartu, 1992.
13. **Tõnu Reinot**. The kinetics of polariton luminescence, energy transfer and relaxation in anthracene. Tartu, 1992.
14. **Toomas Rõõm**. Paramagnetic H^{2-} and F^+ centers in CaO crystals: spectra, relaxation and recombination luminescence. Tallinn, 1993.
15. **Erko Jalviste**. Laser spectroscopy of some jet-cooled organic molecules. Tartu, 1993.
16. **Alvo Aabloo**. Studies of crystalline celluloses using potential energy calculations. Tartu, 1994.
17. **Peeter Paris**. Initiation of corona pulses. Tartu, 1994.
18. **Павел Рубин**. Локальные дефектные состояния в CuO_2 плоскостях высокотемпературных сверхпроводников. Тарту, 1994.
19. **Olavi Ollikainen**. Applications of persistent spectral hole burning in ultrafast optical neural networks, time-resolved spectroscopy and holographic interferometry. Tartu, 1996.
20. **Ülo Mets**. Methodological aspects of fluorescence correlation spectroscopy. Tartu, 1996.
21. **Mikhail Danilkin**. Interaction of intrinsic and impurity defects in CaS:Eu luminophors. Tartu, 1997.

22. **Ирина Кудрявцева**. Создание и стабилизация дефектов в кристаллах KBr, KCl, RbCl при облучении ВУФ-радиацией. Тарту, 1997.
23. **Andres Osvet**. Photochromic properties of radiation-induced defects in diamond. Tartu, 1998.
24. **Jüri Örd**. Classical and quantum aspects of geodesic multiplication. Tartu, 1998.
25. **Priit Sarv**. High resolution solid-state NMR studies of zeolites. Tartu, 1998.
26. **Сергей Долгов**. Электронные возбуждения и дефектообразование в некоторых оксидах металлов. Тарту, 1998.
27. **Kaupo Kukli**. Atomic layer deposition of artificially structured dielectric materials. Tartu, 1999.
28. **Ivo Heinmaa**. Nuclear resonance studies of local structure in $RBa_2Cu_3O_{6+x}$ compounds. Tartu, 1999.
29. **Aleksander Shelkan**. Hole states in CuO_2 planes of high temperature superconducting materials. Tartu, 1999.
30. **Dmitri Nevedrov**. Nonlinear effects in quantum lattices. Tartu, 1999.
31. **Rein Ruus**. Collapse of 3d (4f) orbitals in 2p (3d) excited configurations and its effect on the x-ray and electron spectra. Tartu, 1999.
32. **Valter Zazubovich**. Local relaxation in incommensurate and glassy solids studied by Spectral Hole Burning. Tartu, 1999.
33. **Indrek Reimand**. Picosecond dynamics of optical excitations in GaAs and other excitonic systems. Tartu, 2000.
34. **Vladimir Babin**. Spectroscopy of exciton states in some halide macro- and nanocrystals. Tartu, 2001.
35. **Toomas Plank**. Positive corona at combined DC and AC voltage. Tartu, 2001.
36. **Kristjan Leiger**. Pressure-induced effects in inhomogeneous spectra of doped solids. Tartu, 2002.
37. **Helle Kaasik**. Nonperturbative theory of multiphonon vibrational relaxation and nonradiative transitions. Tartu, 2002.
38. **Tõnu Laas**. Propagation of waves in curved spacetimes. Tartu, 2002.
39. **Rünno Lõhmus**. Application of novel hybrid methods in SPM studies of nanostructural materials. Tartu, 2002.
40. **Kaido Reivelt**. Optical implementation of propagation-invariant pulsed free-space wave fields. Tartu, 2003.
41. **Heiki Kasemägi**. The effect of nanoparticle additives on lithium-ion mobility in a polymer electrolyte. Tartu, 2003.
42. **Villu Repän**. Low current mode of negative corona. Tartu, 2004.
43. **Алексей Котлов**. Оксианионные диэлектрические кристаллы: зонная структура и электронные возбуждения. Tartu, 2004.
44. **Jaak Talts**. Continuous non-invasive blood pressure measurement: comparative and methodological studies of the differential servo-oscillometric method. Tartu, 2004.
45. **Margus Saal**. Studies of pre-big bang and braneworld cosmology. Tartu, 2004.

46. **Eduard Gerškevitš**. Dose to bone marrow and leukaemia risk in external beam radiotherapy of prostate cancer. Tartu, 2005.
47. **Sergey Shchemelyov**. Sum-frequency generation and multiphoton ionization in xenon under excitation by conical laser beams. Tartu, 2006.
48. **Valter Kiisk**. Optical investigation of metal-oxide thin films. Tartu, 2006.
49. **Jaan Aarik**. Atomic layer deposition of titanium, zirconium and hafnium dioxides: growth mechanisms and properties of thin films. Tartu, 2007.
50. **Astrid Rekker**. Colored-noise-controlled anomalous transport and phase transitions in complex systems. Tartu, 2007.
51. **Andres Punning**. Electromechanical characterization of ionic polymer-metal composite sensing actuators. Tartu, 2007.
52. **Indrek Jõgi**. Conduction mechanisms in thin atomic layer deposited films containing TiO_2. Tartu, 2007.
53. **Aleksei Krasnikov**. Luminescence and defects creation processes in lead tungstate crystals. Tartu, 2007.
54. **Küllike Rägo**. Superconducting properties of MgB_2 in a scenario with intra- and interband pairing channels. Tartu, 2008.
55. **Els Heinsalu**. Normal and anomalously slow diffusion under external fields. Tartu, 2008.
56. **Kuno Kooser**. Soft x-ray induced radiative and nonradiative core-hole decay processes in thin films and solids. Tartu, 2008.
57. **Vadim Boltrushko**. Theory of vibronic transitions with strong nonlinear vibronic interaction in solids. Tartu, 2008.
58. **Andi Hektor**. Neutrino Physics beyond the Standard Model. Tartu, 2008.
59. **Raavo Josepson**. Photoinduced field-assisted electron emission into gases. Tartu, 2008.
60. **Martti Pärs**. Study of spontaneous and photoinduced processes in molecular solids using high-resolution optical spectroscopy. Tartu, 2008.
61. **Kristjan Kannike**. Implications of neutrino masses. Tartu, 2008.
62. **Vigen Issahhanjan**. Hole and interstitial centres in radiation-resistant MgO single crystals. Tartu, 2008.
63. **Veera Krasnenko**. Computational modeling of fluorescent proteins. Tartu, 2008.
64. **Mait Müntel**. Detection of doubly charged higgs boson in the CMS detector. Tartu, 2008.
65. **Kalle Kepler**. Optimisation of patient doses and image quality in diagnostic radiology. Tartu, 2009.
66. **Jüri Raud**. Study of negative glow and positive column regions of capillary HF discharge. Tartu, 2009.
67. **Sven Lange**. Spectroscopic and phase-stabilisation properties of pure and rare-earth ions activated ZrO_2 and HfO_2. Tartu, 2010.
68. **Aarne Kasikov**. Optical characterization of inhomogeneous thin films. Tartu, 2010.
69. **Heli Valtna-Lukner**. Superluminally propagating localized optical pulses. Tartu, 2010.

70. **Artjom Vargunin**. Stochastic and deterministic features of ordering in the systems with a phase transition. Tartu, 2010.
71. **Hannes Liivat**. Probing new physics in e+e− annihilations into heavy particles via spin orientation effects. Tartu, 2010.
72. **Tanel Mullari**. On the second order relativistic deviation equation and its applications. Tartu, 2010.
73. **Aleksandr Lissovski**. Pulsed high-pressure discharge in argon: spectroscopic diagnostics, modeling and development. Tartu, 2010.
74. **Aile Tamm**. Atomic layer deposition of high-permittivity insulators from cyclopentadienyl-based precursors. Tartu, 2010.
75. **Janek Uin**. Electrical separation for generating standard aerosols in a wide particle size range. Tartu, 2011.
76. **Svetlana Ganina**. Hajusandmetega ülesanded kui üks võimalus füüsikaõppe efektiivsuse tõstmiseks. Tartu, 2011
77. **Joel Kuusk**. Measurement of top-of-canopy spectral reflectance of forests for developing vegetation radiative transfer models. Tartu, 2011.
78. **Raul Rammula**. Atomic layer deposition of HfO_2 – nucleation, growth and structure development of thin films. Tartu, 2011.
79. **Сергей Наконечный**. Исследование электронно-дырочных и интерстициал-вакансионных процессов в монокристаллах MgO и LiF методами термоактивационной спектроскопии. Тарту, 2011.
80. **Niina Voropajeva**. Elementary excitations near the boundary of a strongly correlated crystal. Tartu, 2011.
81. **Martin Timusk**. Development and characterization of hybrid electro-optical materials. Tartu, 2012, 106 p.
82. **Merle Lust**. Assessment of dose components to Estonian population. Tartu, 2012, 84 p.
83. **Karl Kruusamäe**. Deformation-dependent electrode impedance of ionic electromechanically active polymers. Tartu, 2012, 128 p.
84. **Liis Rebane**. Measurement of the $W \to \tau\nu$ cross section and a search for a doubly charged Higgs boson decaying to τ-leptons with the CMS detector. Tartu, 2012, 156 p.
85. **Jevgeni Šablonin**. Processes of structural defect creation in pure and doped MgO and NaCl single crystals under condition of low or super high density of electronic excitations. Tartu, 2013, 145 p.
86. **Riho Vendt**. Combined method for establishment and dissemination of the international temperature scale. Tartu, 2013, 108 p.
87. **Peeter Piksarv**. Spatiotemporal characterization of diffractive and non-diffractive light pulses. Tartu, 2013, 156 p.
88. **Anna Šugai**. Creation of structural defects under superhigh-dense irradiation of wide-gap metal oxides. Tartu, 2013, 108 p.
89. **Ivar Kuusik**. Soft X-ray spectroscopy of insulators. Tartu, 2013, 113 p.
90. **Viktor Vabson**. Measurement uncertainty in Estonian Standard Laboratory for Mass. Tartu, 2013, 134 p.

91. **Kaupo Voormansik**. X-band synthetic aperture radar applications for environmental monitoring. Tartu, 2014, 117 p.
92. **Deivid Pugal**. hp-FEM model of IPMC deformation. Tartu, 2014, 143 p.
93. **Siim Pikker**. Modification in the emission and spectral shape of photo-stable fluorophores by nanometallic structures. Tartu, 2014, 98 p.
94. **Mihkel Pajusalu**. Localized Photosynthetic Excitons. Tartu, 2014, 183 p.
95. **Taavi Vaikjärv**. Consideration of non-adiabaticity of the Pseudo-Jahn-Teller effect: contribution of phonons. Tartu, 2014, 129 p.
96. **Martin Vilbaste**. Uncertainty sources and analysis methods in realizing SI units of air humidity in Estonia. Tartu, 2014, 111 p.
97. **Mihkel Rähn**. Experimental nanophotonics: single-photon sources- and nanofiber-related studies. Tartu, 2015, 107 p.
98. **Raul Laasner**. Excited state dynamics under high excitation densities in tungstates. Tartu, 2015, 125 p.
99. **Andris Slavinskis**. EST Cube-1 attitude determination. Tartu, 2015, 104 p.
100. **Karlis Zalite**. Radar Remote Sensing for Monitoring Forest Floods and Agricultural Grasslands. Tartu, 2016, 124 p.
101. **Kaarel Piip**. Development of LIBS for *in-situ* study of ITER relevant materials. Tartu, 2016, 93 p.
102. **Kadri Isakar**. ^{210}Pb in Estonian air: long term study of activity concentrations and origin of radioactive lead. Tartu, 2016, 107 p.
103. **Artur Tamm**. High entropy alloys: study of structural properties and irradiation response. Tartu, 2016, 115 p.
104. **Rasmus Talviste**. Atmospheric-pressure He plasma jet: effect of dielectric tube diameter. Tartu, 2016, 107 p.
105. **Andres Tiko**. Measurement of single top quark properties with the CMS detector. Tartu, 2016, 161 p.
106. **Aire Olesk**. Hemiboreal Forest Mapping with Interferometric Synthetic Aperture Radar. Tartu, 2016, 121 p.
107. **Fred Valk**. Nitrogen emission spectrum as a measure of electric field strength in low-temperature gas discharges. Tartu, 2016, 149 p.
108. **Manoop Chenchiliyan**. Nano-structural Constraints for the Picosecond Excitation Energy Migration and Trapping in Photosynthetic Membranes of Bacteria. Tartu, 2016, 115p.
109. **Lauri Kaldamäe**. Fermion mass and spin polarisation effects in top quark pair production and the decay of the higgs boson. Tartu, 2017, 104 p.
110. **Marek Oja**. Investigation of nano-size α- and transition alumina by means of VUV and cathodoluminescence spectroscopy. Tartu, 2017, 89 p.
111. **Viktoriia Levushkina**. Energy transfer processes in the solid solutions of complex oxides. Tartu, 2017, 101 p.
112. **Mikk Antsov**. Tribomechanical properties of individual 1D nanostructures: experimental measurements supported by finite element method simulations. Tartu, 2017, 101 p.
113. **Hardi Veermäe**. Dark matter with long range vector-mediated interactions. Tartu, 2017, 137 p.

114. **Aris Auzans**. Development of computational model for nuclear energy systems analysis: natural resources optimisation and radiological impact minimization. Tartu, 2018, 138 p.
115. **Aleksandr Gurev**. Coherent fluctuating nephelometry application in laboratory practice. Tartu, 2018, 150 p.
116. **Ardi Loot**. Enhanced spontaneous parametric downconversion in plasmonic and dielectric structures. Tartu, 2018, 164 p.
117. **Andreas Valdmann**. Generation and characterization of accelerating light pulses. Tartu, 2019, 85 p.
118. **Mikk Vahtrus**. Structure-dependent mechanical properties of individual one-dimensional metal-oxide nanostructures. Tartu, 2019, 110 p.
119. **Ott Vilson**. Transformation properties and invariants in scalar-tensor theories of gravity. Tartu, 2019, 183 p.
120. **Indrek Sünter**. Design and characterisation of subsystems and software for ESTCube-1 nanosatellite. Tartu, 2019, 195 p.
121. **Marko Eltermann**. Analysis of samarium doped TiO_2 optical and multiresponse oxygen sensing capabilities. Tartu, 2019, 113 p.
122. **Kalev Erme**. The effect of catalysts in plasma oxidation of nitrogen oxides. Tartu, 2019, 114 p.
123. **Sergey Koshkarev**. A phenomenological feasibility study of the possible impact of the intrinsic heavy quark (charm) mechanism on the production of doubly heavy mesons and baryons. Tartu, 2020, 134 p.
124. **Kristi Uudeberg**. Optical Water Type Guided Approach to Estimate Water Quality in Inland and Coastal Waters. Tartu, 2020, 222 p.
125. **Daniel Blixt**. Hamiltonian analysis of covariant teleparallel theories of gravity. Tartu, 2021, 142 p.
126. **Ulbossyn Ualikhanova**. Gravity theories based on torsion: theoretical and observational constraints. Tartu, 2021, 154 p.
127. **Iaroslav Iakubivskyi**. Nanospacecraft for Technology Demonstration and Science Missions. Tartu, 2021, 177 p.
128. **Heido Trofimov**. Polluted clouds at air pollution hot spots help to better understand anthropogenic impacts on Earth's climate. Tartu, 2022, 96 p.
129. **Ott Rebane**. *In situ* non-contact sensing of microbiological contamination by fluorescence spectroscopy. Tartu, 2022, 157 p.
130. **Juhan Saaring**. Ultrafast Relaxation Processes in Ternary Hexafluorides Studied under Synchrotron Radiation Excitation. Tartu, 2022, 106 p.
131. **Ahmet Ilker Topuz**. Quantitative and qualitative investigations for muon scattering tomography via GEANT4 simulations: A computational study. Tartu, 2023, 163 p.
132. **Nico Benincasa**. Phase transitions and gravitational waves in models of dark matter. Tartu, 2023, 206 p.
133. **Kaja Pae**. Electron-phonon interactions in local degenerate electronic states in solids. Tartu, 2024, 201 p.
134. **Kristjan Müürsepp**. Phenomenological implications of Standard Model extensions. Tartu, 2024, 136 p.

135. **Ye Wang**. Investigating the properties of metal surfaces under high electric fields based on ab initio calculations. Tartu, 2024, 107 p.
136. **Laxmipriya Pati**. The effects of non-Riemannian connection in teleparallel gravity. Tartu, 2025, 172 p.
137. **Débora Aguiar Gomes**. Theoretical and astrophysical aspects of extended general relativity. Tartu, 2025, 169 p.
138. **Mina Hajizadeh Omaslanolya**. Structure and dynamics of photoactive proteins studied by (in situ-) neutron scattering methods. Tartu, 2025, 150 p.
139. **Aditya Savio Paul**. Advancing the study of small solar system bodies through multi-agent mapping and characterization. Tartu, 2025, 244 p.
140. **Sanu Bifal Maji**. Synthesis and luminescence investigation of nano-particles doped with Pr^{3+} ions in selected fluoride and phosphate hosts. Tartu, 2025, 114 p.
141. **Ernest Michael Priidik Gallagher**. On the internal gauge theory analogy to the Cartan Khronon theory of gravity. Tartu, 2026, 221 p.
142. **Maria Naeem**. First order electroweak radiative corrections to the decay of the polarised *W* boson. Tartu, 2026, 236 p.
143. **Konstantinos Pallikaris**. Novel black holes in Einstein gravity. Tartu, 2026, 133 p.
144. **Aleksei Kubarski**. Dynamical symmetry breaking and dark matter. Tartu, 2026, 133 p.
145. **Lucy Zheng**. Cartan Khronon – Real space-time structure. Tartu, 2026, 193 p.